Strong aerosol indirect radiative effect from dynamic-driven diurnal variations of cloud water adjustments

Jiayi Li[1]~~‡,~~[+], Yang Wang[1]~~‡,~~[+], Jiming Li[1*], Weiyuan Zhang[1], Lijie Zhang[1], Yuan Wang[1]

[1] Collaborative Innovation Center for Western Ecological Safety, College of Atmospheric Sciences, Lanzhou University, Lanzhou 730000, China.

Correspondence to: Jiming Li (lijiming@lzu.edu.cn)

~~‡~~[+] These authors contributed equally to this work.

Abstract. Aerosol-cloud interaction (ACI) ~~is the critical yet most uncertain process~~remains a key uncertainty in ~~future~~ climate projections. A major challenge is that the sign and magnitude of cloud liquid water path (LWP) response to aerosol perturbations (represented by cloud droplet number concentration, N_d) at different temporal and spatial scales are highly variable, but potential microphysical-dynamical mechanisms are still unclear, especially at a diurnal scale. ~~Here, robust observational evidence from geostationary satellite reveals that~~Here, geostationary observations were conducted in two distinct cloud regions: the stratocumulus region off the western Australia and clouds over the East China Sea characterized by a transition from stratocumulus to cumulus under strong anthropogenic influences. In contrast to the commonly observed inverted-V N_d-LWP relationship, LWP increases at high N_d (> ~300 cm^{-3}) in the ECS, exhibiting a V shape. Our analysis indicates this unique V shape arises from large-scale meteorological covariations (e.g. cold air advection), which lead to increases in both LWP and N_d. Furthermore, the diurnal variation of LWP adjustments is driven primarily by diurnal-related boundary layer decoupling and cloud-top entrainment. ~~Strikingly, these~~The diurnal LWP adjustments exhibit a distinct regional pattern associated with cloud regimes. ~~We find~~The results indicate that ~~the cooling effect of LWP adjustments would be underestimated by up to 89% in study regions if~~ neglecting ~~their~~ diurnal variations~~, leading to a further 20% offset~~ of LWP adjustments leads to an underestimation (up to 89%) of ~~Twomey effect, thus biasing~~the cooling effect induced by changes in cloud albedo due to aerosol ~~indirect effect toward~~perturbations in the AUW. The bias spans from a 24% overestimation to a ~~warming direction.~~40% underestimation in the ECS. Our findings highlight the key role of diurnal ~~variation~~variations of ACI in reducing the uncertainty in climate projections.

1 Introduction

Marine low-level clouds (MLCs), which cover one-third of the global ocean (Klein and Hartmann, 1993), exert a strong cooling effect by reflecting the incoming solar radiation back into space (Jiang et al., 2023). ~~Their~~Cloud reflectivity to solar radiation is highly sensitive to atmospheric aerosol concentrations~~ because~~. Because aerosols can serve as the cloud condensation nuclei (CCN~~) to~~), which modify ~~the mediated~~key microphysical variables ~~(e.g.~~ such as cloud droplet number concentrations~~,~~ (N_d~~;~~) and droplet effective radius~~,~~ (r_e~~) of~~). For a given cloud liquid water content, aerosol-~~cloud interactions (ACI). ACI contributes the largest uncertainty of aerosol radiative forcing and future climate projections. Aerosol-~~induced increases in CCN can enhance N_d and hence reduce r_e, boosting cloud albedo~~ while holding cloud liquid water content (the Twomey effect)~~ (Twomey, 1977)~~.~~, which is known as cloud albedo effect, being an important component of aerosol-cloud interactions (ACI). Additional alterations in cloud microphysics may arise from changes in the quantity of liquid water or cloud cover that are induced by aerosol variations. These changes can lead to rapid adjustments within the cloud in response to aerosol perturbations, ~~indicating that the impact of aerosols on cloud properties is multifaceted (Bellouin et al., 2020)~~which is another crucial component of ACI (Bellouin et al., 2020). For example, it has been documented that liquid water path (LWP) can either increase due to precipitation suppression (positive LWP adjustments) (Albrecht, 1989) or decrease due to entrainment feedbacks (negative LWP adjustments) (Ackerman et al., 2004; Bretherton et al., 2007; Small et al., 2009). While the Twomey effect is well-recognized, however, LWP adjustments are highly uncertain as the least understood and most poorly quantified in all climate forcing (IPCC, 2023).

These large uncertainties in LWP adjustments are generally attributed to the complex interplay of microphysical-dynamical conditions and aerosol loading (represented by N_d) that vary with different temporal and spatial scales (Bender et al., 2019; Chen et al., 2014; Glassmeier et al., 2021; Gryspeerdt et al., 2022a). Numerous observational studies have been carried out to understand the extent of this variability and uncertainties of LWP adjustments, with the aim of constraining model simulations ~~(Gryspeerdt et al., 2019, 2021; Rosenfeld et al., 2019; Trofimov et al., 2020; Wilcox, 2010)~~(Gryspeerdt et al., 2019, 2021; Rosenfeld et al., 2019; Trofimov et al., 2020; Wilcox, 2010). These investigations have spanned various regions and targets, revealing diverse cloud responses attributable to the varied mechanisms of LWP adjustments. In addition, it has been confirmed that analysis methods, sampling strategies, and ~~meteorology~~meteorological covariations could be ~~a~~another considerable~~ other~~ source of uncertainty in LWP adjustments (Chen et al., 2014; Gryspeerdt et al., 2022b; Rosenfeld et al., 2019, 2023). Here, we focus on the time-dependence of LWP adjustments (i.e., diurnal variations) as it is associated with both sampling strategies and ~~meteorology~~meteorological covariations. It has been established that marine cloud properties and the cloud-topped marine boundary layer exhibit prominent diurnal variations in response to solar radiation, which are closely related to their regional dependence (Duynkerke and Hignett, 1993; Wood et al., 2002). The microphysical-dynamical boundary layer feedback, which generally covaries with the regional diurnal cycle, could augment or weaken the LWP adjustments and thus lead to the diurnal variation of LWP adjustments with broad spreads and even different signs. This means that a one-size-fits-all approach to global-mean LWP adjustments may not provide a robust constraint, given the regional and temporal mechanisms at play (Michibata et al., 2016). Additionally, the microphysical-dynamical mechanisms behind are complex and still poorly understood (Feingold et al., 2024). This drives the speculation that the diurnal variations of LWP adjustments could be one of the most significant yet overlooked sources of uncertainty of ACI.

However, to date, a majority of studies have relied on observations from polar-orbiting satellites to investigate the spatial distribution and long-term variations of N_d (Bennartz and Rausch, 2017; Li et al., 2018; McCoy et al., 2018), which are insufficient to depict the time-dependent nature of LWP adjustments. Based on Himawari-8 geostationary satellite, the diurnal variations of cloud microphysical properties and LWP adjustments in two typical regions~~ as selected~~, and the associated influencing factors and mechanisms are presented in this study. Our research aims to expand our understanding of the influence of meteorological factors, initial aerosol states (~~specially~~especially N_d), and the covariance between meteorology and aerosols on cloud LWP, gaining a comprehensive understanding of the diurnal variations in LWP adjustments, which is a highly time-dependent variable lacking quantification, in conjunction with shifts in regional meteorological conditions.

2 Data and Methods

~~Our analysis focuses on 1° × 1° non-precipitation marine low-level cloud samples, aggregated from filtered pixel-level satellite data. We aim to avoid the impact of precipitation on retrieval of N_d and focus only on the development of clouds in response to aerosol loading associated with microphysical-dynamical conditions over two selected regions. One is located in the west of Australia (25º-35ºS, 95º-105ºE, AUW). The other is in the East China Sea (20º-30ºN, 120º-130ºE, ECS), as shown in Figure S1 in Supplementary Materials.~~

Our analysis focuses on 1° × 1° marine low-level cloud samples, aggregated from filtered pixel-level satellite data. Within the sight of Himawari-8, we selected two cloud regions with significantly different environmental backgrounds (see Fig. S1 in Supplementary Materials). One is a remote stratocumulus region located in the west of Australia (AUW: 25º-35ºS, 95º-105ºE) (Klein and Hartmann, 1993). The other is in the East China Sea (ECS: 20º-30ºN, 120º-130ºE), which is significantly impacted by anthropogenic aerosols and characterized by Sc to Cu transition (Long et al., 2020). The comparison between the two regions allows us to explore the regional differences of LWP adjustments and their potential driving mechanisms. In total, we collected 480189 cloud samples in the AUW and 173181 cloud samples in the ECS using a 4-year (2016-2019) hourly record from SatCORPS Himawari-8.

2.1 N_d retrieval based on geostationary satellite product

In this study, 4 years (2016-2019) of hourly cloud microphysical properties data from the Satellite Cloud and Radiation Property retrieval System (SatCORPS) Clouds and the Earth's Radiant Energy System (CERES) Geostationary Satellite (GEO) Edition 4 Himawari-8 over the Northern Hemisphere (NH) (Southern Hemisphere (SH)) Version 1.2 data product (CER_GEO_ED4_HIM08_NH_V01.2, CER_GEO_ED4_HIM08_SH_V01.2) were collected ~~(NASA/LARC/SD/ASDC, 2018b, a).~~(NASA/LARC/SD/ASDC, 2018b, a). The datasets are derived from the Advanced Himawari Imagers (AHI) on Himawari-8 geostationary satellite, using the Langley Research Center (LARC)s SatCORPS algorithms in support of the CERES project (Minnis et al., 2021; Trepte et al., 2019)~~. The retrievals are at 2-km resolution (at nadir) and are sub-sampled to 6 km. The sub-sampled resolution meets the needs of the CERES project without having a data implosion. The cloud optical thickness (CLOT), cloud effective radius (r_e) and cloud-top temperature (CLTT) from the SatCORPS product during the daytime were used to retrieve N_d in our study. Other cloud properties such as cloud-top height (CLTH), cloud base height (CLBH) and cloud thickness (H) were used in further analysis. The SatCORPS is based on the CERES Ed4 cloud retrieval~~

~~algorithm, providing more accurate CLTH and H parameterizations (Minnis et al., 2011, 2021). Briefly, CLTH is estimated as the altitude where the cloud-top temperature (CLTT) occurs in the temperature profile. The temperature profile is provided by CERES Meteorology, Ozone, and Aerosol (CERES MOA) dataset. CLTT is derived from an empirical parameterization of cloud-top emissivity at channel 4 and cloud effective temperature. H is computed using empirical formulas with τ: $H = 0.39 \ln \tau - 0.01$ for liquid clouds. CLBH is directly obtained by subtracting H from CLTH.~~

~~The~~ . The retrievals are at 2-km resolution (at nadir) and are sub-sampled to 6 km. The sub-sampled resolution meets the needs of the CERES project without having a data implosion. The cloud optical thickness (CLOT), cloud effective radius (r_e) and cloud-top temperature (CLTT) from the SatCORPS product during the daytime were used to calculate N_d in our study. Other cloud properties such as cloud-top height (CLTH), cloud base height (CLBH) and cloud thickness (H) were used in further analysis. The SatCORPS product is based on the CERES Ed4 cloud retrieval algorithm (Minnis et al., 2021), which provides more accurate parameterizations of CLTH and H than the CERES Edition 2 retrieval algorithm (Minnis et al., 2011). Briefly, for boundary layer clouds, CLTH is retrieved using a lapse rate method: $\Gamma_b = (CET - T_0)/(\mathrm{CLTH} - Z_0)$ (Sun-Mack et al., 2014). Cloud effective temperature (CET) was estimated from the Infrared Window (IRW) channel. Z_0 denotes the surface elevation and T_0 is the sea surface temperature. H is computed using empirical formulas with τ: $\mathrm{H} = 0.39 \ln \tau - 0.01$ for liquid clouds. CLBH is directly obtained by subtracting H from CLTH.

SatCORPS ~~retrievals provide~~ cloud droplet effective radius (r_e) ~~in~~is primarily estimated from the 3.9 µm near-infrared band (Kang et al., 2021), which is closest to the cloud top with less bias in further calculation of N_d (Grosvenor et al., 2018). N_d ~~can be~~is estimated as (Bennartz, 2007):

$$N_d = \frac{\sqrt{5}}{2\pi k}\left(\frac{f_{ad} c_{\omega} \tau}{Q \rho_w {r_e}^5}\right)^{\frac{1}{2}} \tag{1}$$

where τ represents cloud optical depth and ρ_w is liquid water density. The extinction efficiency factor $Q \approx 2$~~, as Q relies less on the size parameter in near-infrared~~. k, related to droplet size distribution, is set as 0.8 for maritime cloud (Martin et al., 1994; Painemal and Zuidema, 2011). c_w represents the condensation rate determined by temperature in cloud (here is the cloud-top temperature from SatCORPS). A constant adiabatic value (f_{ad}) of 0.8 is used to represent the deviation from the adiabatic profile (Bennartz, 2007). This is the most common method to derive N_d from passive satellite observations (Bennartz, 2007; Bennartz and Rausch, 2017; Li et al., 2018; McCoy et al., 2018) and has been validated as a reliable technique for observing changes in long-term variations of N_d (Boers et al., 2006). Li et al. (2018) demonstrated that passive satellite N_d retrievals exhibit strong consistency with active satellite retrievals. The SatCORPS Himawari-8 retrievals agree well with in-situ observations according to Kang et al. (2021). In this study, the LWP from SatCORPS is calculated as $\frac{5}{9}\rho_w \tau r_e$ in sub-adiabatic conditions, following the method by Wood and Hartmann (2006). The combination of these two retrieval methods of N_d and LWP has been widely used in the satellite investigations of LWP ~~adjustment~~adjustments (Fons et al., 2023; Gryspeerdt et al., 2019; Qiu et al., 2023; Smalley et al., 2024).

Several sampling strategies were adopted in this study to select cloud pixels to ~~meet the above retrieval assumptions~~reduce uncertainties (Grosvenor et al., 2018; Gryspeerdt et al., 2019; Li et al., 2018). Only pixels in the liquid phase with cloud-top temperature warmer than 268 K under 3.2 km were included. To maintain consistency with previous studies (Bennartz and Rausch, 2017; Li et al., 2018), we adopted 268 K as the threshold of CLTT for liquid clouds, rather than 273 K. In fact, 96% (97%) of the samples exhibited CLTT above 273 K in the AUW (ECS) region. Therefore, the threshold has a negligible impact on the overall results. The lower bounds of r_e (τ) were set as 4 μm (4) to reduce uncertainties. Moreover, pixels with solar zenith angles larger than 65° were excluded. Filtered data ~~was~~were used to calculate N_d and then aggregated to a 1° × 1° grid. Each grid containing at least 30 pixels is considered a cloud sample. On average, each grid contains 83 (87) pixels in the AUW (ECS) region.

We followed the ~~previous~~above methods to filter cloud pixels~~. But this classification~~, which only ~~limits~~limit cloud top properties and cloud phase, inevitably including different cloud regimes, such as low-level cumulus clouds. This might introduce uncertainties as cumulus clouds and stratocumulus clouds have different adiabatic properties~~ but we have set the adiabatic rate as a constant value in the retrieval process. Uncertainties may occur as f_{ad} varies with cloud depth (Grosvenor et al., 2018; Min et al., 2012). As acquiring hourly f_{ad} on a global scale is difficult, to date, studies investigating diurnal variations~~, but we have set f_{ad} as a constant value in N_d calculations. Small et al. (2013) found that the f_{ad} of cumulus clouds showed no significant variation with height, whereas Wood (2005) observed that the adiabaticity in stratocumulus clouds decreased from cloud base to cloud top. The difference in departures from adiabaticity between cumulus and stratocumulus stems from their different entrainment processes. Stratocumulus clouds are primarily influenced by the entrainment of dry air at cloud top (Mellado, 2017). In contrast, cumulus clouds are dominated by lateral entrainment (Heus et al., 2008). Uncertainties may also occur as f_{ad} varies with cloud depth (Grosvenor et al., 2018; Min et al., 2012; Wang et al., 2021). As acquiring hourly f_{ad} on a global scale is rather difficult, to date, studies investigating diurnal variations of LWP adjustments based on geostationary satellites continue to employ a constant f_{ad} value (Fons et al., 2023; Qiu et al., 2024; Smalley et al., 2024). ~~Also, the choices of constant k might introduce bias into the retrieval of N_d.~~Also, the choices of a constant k might introduce bias into the retrieval of N_d (Grosvenor et al., 2018). Studies have found that k parameter varied with the height within cloud and cloud types ~~(Brenguier et al., 2011; Martin et al., 1994; Painemal and Zuidema, 2011)~~(Brenguier et al., 2011; Martin et al., 1994; Painemal and Zuidema, 2011). ~~Since the bias caused by the retrieval contributes equally to all samples, it may change the magnitude of variables without changing the diurnal patterns or the mechanisms behind them. Consequently, the above uncertainties will not greatly affect the conclusions of this paper~~This indicates that the presence of diurnal variations in k and f_{ad} (e.g., hourly changes in entrainment rate can modify f_{ad}) introduces further bias. The resulting uncertainties warrant further in situ observation to improve the accuracy.

To minimize the influence of precipitation~~, particularly the bias introduced in~~ on N_d and LWP retrievals~~ due to invalidating the adiabatic (or sub-adiabatic) assumption, only non-precipitating clouds are discussed in this study. Therefore~~, GPM IMERG Final Precipitation L3 Half Hourly 0.1 degree x 0.1 degree V07 (GPM_3IMERGHH) was used ~~as a precipitation criterion~~ (Huffman et al., 2020)~~.~~. Cloud samples were included in the analysis only if the GPM_3IMERGHH precipitation rate equals 0 mm/hr in a 1° × 1° grid. To align these two satellite products, SatCORPS cloud pixels within each 0.1° grid of

GPM_3IMERGHH are assigned the same precipitation value. ~~Cloud samples are regarded as~~Considering the limited ability of GPM to detect light precipitation and drizzle, we additionally applied a r_e = 14 μm threshold to distinguish between drizzle scenes and non-~~precipitation only if the GPM_3IMERGHH precipitation rate equals 0 mm/hr in 1° × 1° grid. In total, we collect 480189 cloud samples in AUW and 173181 cloud samples~~drizzle scenes (black lines in ~~ECS using 4-year (2016-2019) hourly record from SatCORPS Himawari-8.~~Fig. 1).

2.2 Quantification of LWP adjustments

To quantify LWP response, ~~both direct and indirect~~two methods have been used in previous studies. The logarithmic relationship between N_d and LWP ($\frac{\partial \ln LWP}{\partial \ln N_d}$) is ~~a direct~~the standard way to quantify LWP sensitivity to aerosol ~~perturbations~~from satellite data, where N_d is considered a proxy of CCN. Another ~~indirect~~ way of describing the ~~variation~~changes of cloud water due to aerosols ($-\frac{\Delta \ln \tau}{\Delta \ln r_e}$) is deduced from the contributions of changes in LWP and r_e to the changes in cloud optical depth ($\frac{\Delta\tau}{\tau} = \frac{\Delta LWP}{LWP} - \frac{\Delta r_e}{r_e}$) (Christensen and Stephens, 2011; Coakley and Walsh, 2002). Whereas the latter method is put forward with a default condition that Δr_e is always negative, it is only applicable to small-scale pollution tracks like industry tracks, volcano tracks or ship tracks, etc. (Rahu et al., 2022; Toll et al., 2019). ~~Therefore, the former method is applied in this study, which has been commonly used in researches on aerosol-cloud interactions based on large-scale satellite observations (e.g., Glassmeier et al., 2021; Gryspeerdt et al., 2019; Rosenfeld et al., 2019)~~Therefore, the former method is applied in this study, which has been commonly used in research on aerosol-cloud interactions based on large-scale satellite observations (e.g. Glassmeier et al., 2021; Gryspeerdt et al., 2019).

LWP adjustment at any given moment is the result of all available data at that moment. The regression slope of N_d and LWP in log-log space ($\frac{\partial \ln LWP}{\partial \ln N_d}$) is calculated on 1° grid scale. ~~Following previous studies (Fons et al., 2023; Rosenfeld et al., 2019), we choose the median LWP in each ln(N_d) bin as the feature point for the entire sample space making the regression more representative of the overall characteristics of all samples (black dots in Figure 1, A and D). Since the relationship between N_d and LWP in non-precipitation clouds shows a non-linear trend in ECS region, turning points in N_d with the lowest LWP are found to characterize LWP adjustments with two different N_d stages (i.e., purple and blue lines in Figure 1D).~~We employed equal-width binning, using the median LWP within each N_d bin to regress the slope. To reduce noise from sparse samples, only bins with more than 50 samples were used to calculate LWP adjustments. Additionally, we tested the equal-sample binning method. The patterns of the N_d-LWP relationship and diurnal variations of LWP adjustments remained robust across different binning methods. The main reason for choosing equal-width binning was to preserve the original physical scale of the samples, avoiding the excessive smoothing of samples with diverse meteorological conditions gathered in a single bin using equal-sample binning (Towers, 2014).

~~**2.3 Reanalysis datasets**~~

~~Aerosol property is represented by the total column extinction optical depth (AOD) at 550 nm from hourly time-averaged 2-dimensional data collection in Modern-Era Retrospective analysis for Research and Applications version 2 (MERRA-2), with a spatial resolution of 0.5° × 0.625° (Buchard et al., 2017). It is interpolated onto a 1° × 1° grid using bilinear interpolation method.~~

2.3 Reanalysis datasets

Aerosol property is represented by the total column extinction optical depth (AOD) at 550 nm from hourly time-averaged 2-dimensional data collection in Modern-Era Retrospective analysis for Research and Applications version 2 (MERRA-2), with a spatial resolution of 0.5° × 0.625° (Buchard et al., 2017). It is interpolated onto a 1° × 1° grid using the bilinear interpolation method.

Meteorological indicators related to cloud microphysical process are ~~either~~ obtained ~~or calculated by~~from ERA5 reanalysis data (Hersbach et al., 2020), including sea surface temperature (SST), lower-tropospheric stability (LTS), relative humidity on 700 hPa and 1000 hPa (RH700 and RH1000), vertical velocity on 700 hPa (omega700~~) and 800 hPa (omega800~~), horizontal wind field on 700 hPa and horizontal temperature advection at the surface (SST_{adv}). The ERA5 is the fifth-generation atmospheric reanalysis of global climate and is produced using the ECMWF's Integrated Forecast System cycle 41r2 with a 4-~~dimension~~dimensional variation assimilation system. Compared to the ERA-Interim, the ERA5 has higher spatial (0.25° × 0.25°) and temporal resolutions (hourly), and the representation of atmospheric processes has been further improved. In this study, the ERA5 reanalysis data is matched to SatCORPS data in the same way as GPM_3IMERGHH.

The LTS is expressed as the difference of potential temperature between 700 hPa and the surface (Klein and Hartmann, 1993). For the horizontal temperature advection at the surface (SST_{adv}), it is expressed in spherical ~~coordinate~~coordinates as Jian et al. (2021) and Qu et al. (2015):

$$\mathrm{SST}_{adv} = -\frac{\mathrm{u}}{\mathrm{R_E}\cos\phi}\frac{\partial \mathrm{SST}}{\partial \lambda} + \frac{\mathrm{v}}{\mathrm{R_E}}\frac{\partial \mathrm{SST}}{\partial \phi} \quad (2)$$

where R_E is the mean Earth radius, SST is the sea surface ~~skin~~ temperature, u and v are the eastward and northward horizontal 10 m wind components, respectively. Φ and λ represent the radians of latitude and longitude. A positive/negative SST_{adv} indicates warm/cold advection, which influences the surface latent and sensible heat fluxes then the moisture transport within the cloud layer and the cloud thickness (George and Wood, 2010) and, consequently, influences the cloud liquid water.

3 Results

3.1 LWP adjustments vary alongside microphysical-dynamical conditions

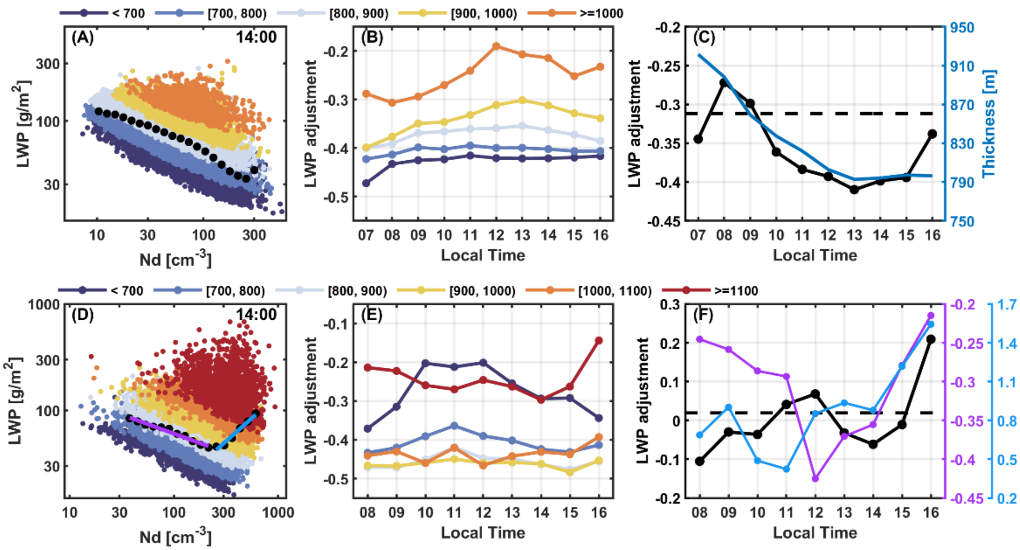

~~**Figure 1. LWP adjustments in log-log spaces and their diurnal patterns in two typical regions (the west of Australia, AUW and the east China sea, ECS).** Non-precipitation cloud samples are scattered in N_d-LWP log space at 1400 LT in (A) AUW and (D) ECS region.~~Figure 1 shows the normalized joint histograms of N_d and LWP in log-log space for all samples in the AUW and ECS regions. The complete pictures of all available daytime~~ Colored dots are samples in different cloud thickness (H) bins (unit: m). Black dots represent the median LWP in each N_d bin. The colored lines are the fits of black dots at different stages in ECS region. Diurnal variations of LWP adjustments binned by H in (B) AUW and (E) ECS regions are shown. Colored lines in (F) are diurnal variations of different stages in (D), while black lines in (C) and (F) are the overall diurnal variations of LWP adjustments in two regions, respectively. The blue line in (C) represents the diurnal variation of H. Dashed lines represent the average LWP adjustments considering diurnal variations, −0.31 for AUW (C) and 0.02 for ECS (F).~~

~~Figure 1 (A and D) shows the scatter plots of N_d-LWP relationship in log-log space for AUW and ECS regions at 1400 LT (local time), respectively. The complete pictures of all available daytime periods are presented in Figure S2. The N_d-LWP relationships show similar patterns during daytime in each region but different results in two regions, with an overall negative adjustment in AUW, meaning that LWP decreases with increased N_d, while the LWP adjustments in ECS region exhibit both positive and negative throughout the day. For non-precipitation clouds, both positive and negative LWP adjustments have been reported (Glassmeier et al., 2021; Michibata et al., 2016; Rosenfeld et al., 2019; Toll et al., 2019) and attributed to different mechanisms (e.g., lifetime effect and entrainment feedbacks) (Michibata et al., 2016). In fact, the sign of LWP adjustment is ultimately subject to the dominant microphysical-dynamical mechanisms for each N_d stage. Before about 300 cm^{-3}, LWP adjustments are dominated by processes at the cloud margins, such as sedimentation-entrainment feedback (Ackerman et al.,~~

~~2004) and evaporation-entrainment feedback (Small et al., 2009), leading to negative LWP adjustments in both regions (Figure 1A and purple line in Figure 1D).~~

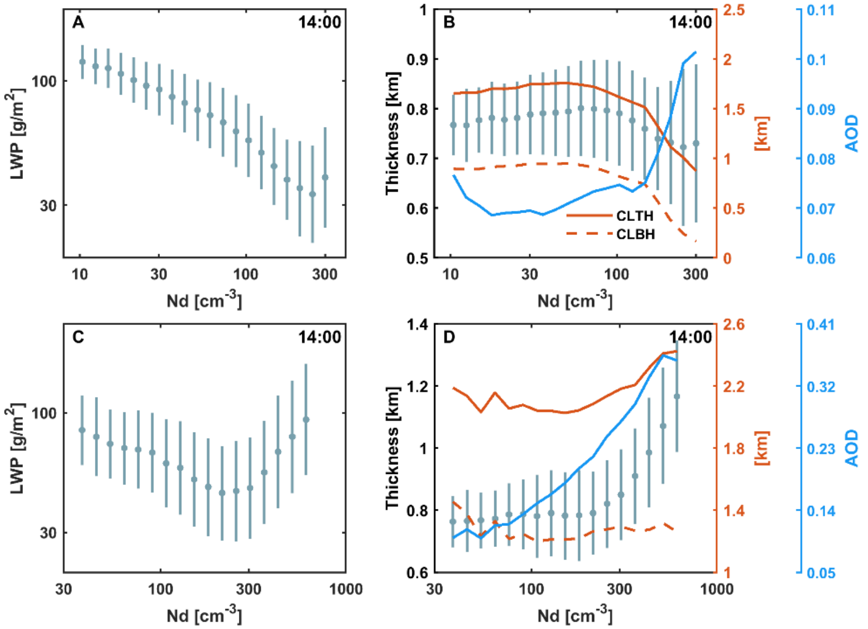

~~**Figure 2. Comparisons between N_d-LWP relationship and N_d-Thickness relationship in two regions.** Relationship between N_d and (A) LWP, (B) cloud thickness in AUW region. Relationship between N_d and (C) LWP, (D) cloud thickness in ECS region. The orange solid and dashed lines show the change of cloud top height (CLTH) and cloud base height (CLBH) with N_d.~~

~~However, LWP begins to rise at high N_d in ECS (blue line in Figure 1D), which is the primary reason causing the overall positive LWP adjustments in this region. Positive sensitivity over ECS has been reported but not fully understood (Bender et al., 2019; Gryspeerdt et al., 2019; Zhang et al., 2021). Michibata et al. (2016) attributed the positive LWP response in non-precipitation clouds over East Asia to the cloud lifetime effect (Albrecht, 1989). Here in ECS region, clouds are heavily affected by anthropogenic aerosols, showing LWP increases with N_d at high N_d (>300 cm^{-3}). This behavior is related to the deepening of cloud depth with aerosols (Figure 2, C and D), indicating warm invigoration by aerosols (Koren et al., 2014).~~

~~The above opposite responses of LWP (either enhanced or decreased) to increasing aerosol loading depends on the environmental conditions and cloud characteristics (Altaratz et al., 2014). On the one hand, they indicated that more droplets delay the collision-coalescence and provide more surface area for condensation, releasing latent heat and promoting cloud vertical development, thus increasing LWP (warm invigoration). On the other hand, more small droplets can be more likely to evaporate due to enhanced entrainment, leading to a decreased LWP (entrainment feedbacks). According to Dagan et al. (2015), the competition between these two processes determines the response of cloud macrophysical properties to aerosols. The N_d-~~

~~LWP relationship in ECS indicates that warm invigoration takes over after around 300 cm^{-3} leading to cloud deepening. Here, we will demonstrate that ECS region is favorable for warm invigoration to occur from three aspects: environmental conditions, cloud regimes and aerosols.~~

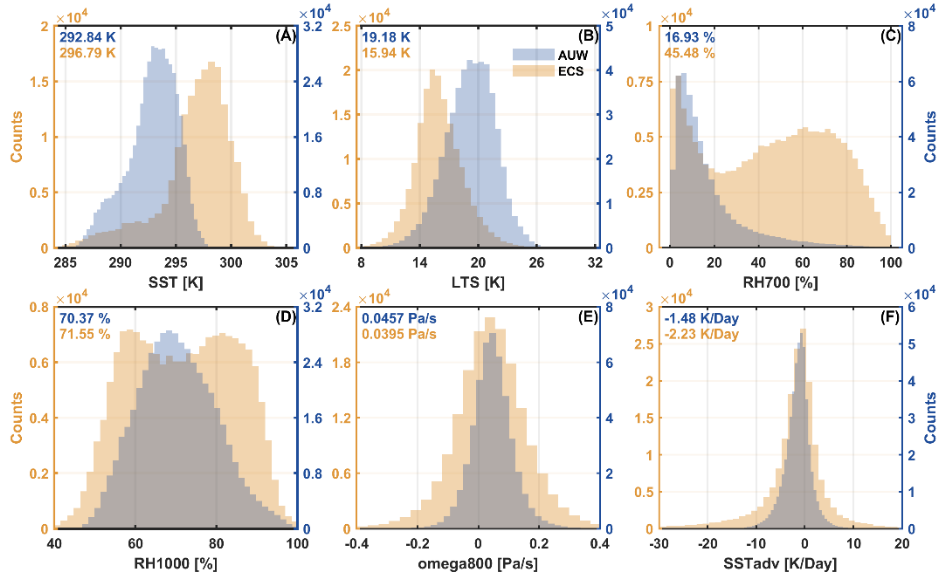

~~Figure 3. 4-year meteorological conditions of non-precipitation clouds in AUW and ECS regions from 2016 to 2019.~~ ~~Histograms of meteorological factors are presented here. The mean values are labeled in the top-left corner. Data are directly or indirectly derived from ERA5. For vertical velocities on 800 hPa (omega800), positive (negative) values indicate downdraft (updraft).~~

~~Although the microphysical-dynamical processes are challenging to observe directly, environmental conditions can be considered as proxies and provide further support for the invigoration effect. The cloud deepening in ECS region is mainly attributed to increasing CLTH (Figure 2D). Unstable boundary layers (low LTS) favor the formation of more convective clouds (Manshausen et al., 2022), while high RH provides moisture for cloud vertical development. The unstable and moist atmosphere in ECS provides such conditions with a mean lower-tropospheric stability (LTS) of 15.94 K and a peak in relative humidity on 700 hPa (RH700) of 70% (Figure 3). Gryspeerdt et al. (2019) also reported this rising behavior at high~~ N_d, ~~especially in moist conditions, consistent with our results noted here. Christensen and Stephens (2011) found elevated cloud-top height from open cell clouds in response to ship pollution in relatively unstable and moist conditions.~~

~~Secondly, the more prevalent convective clouds in the ECS region would be another favorable condition for warm invigoration. Zhang et al. (2021) also attributed the positive LWP adjustments to warm invigoration with the widespread low-level convective clouds (Sc and Cu) in ECS. According to the division from Rosenfeld et al. (2019), we categorize the clouds into three regimes, i.e., Sc (LTS > 18 K), Sc to Cu transition (14 K ≤ LTS ≤ 18 K), and Cu (LTS < 14 K). (Figure 4, G, H and I). We show that clouds in ECS region are dominated by the Sc to Cu transition regime. The formation of this transition regime~~

~~is associated with increasing sea surface temperature (SST) due to “deepening-warming decoupling” (Albrecht et al., 1995; Bretherton and Wyant, 1997). Sc presents over the relatively shallow and stable boundary layer with cooler sea surface along the coast (Figure 4, A and B) and most of Sc may be advected from the southeast Chinese plain (Klein and Hartmann, 1993). According to the cloud advection scheme by Miller et al. (2018), cloud advection can be approximated as a translation of the cloud field with the wind field. The advection height is assumed to correspond to the height of the cloud top. Therefore, we can simply deduce from the wind field on 700 hPa (Figure 4A) that clouds in ECS have the possibility of advection from the Chinese plain in the west. As air moves offshore, MBL deepens and cloud layer decouples with the surface mixed layer over the warmer sea surface. Cu forms in the moist and unstable subcloud layer and rises to the upper cloud layer, resulting in a local cumulus-coupled MBL.~~

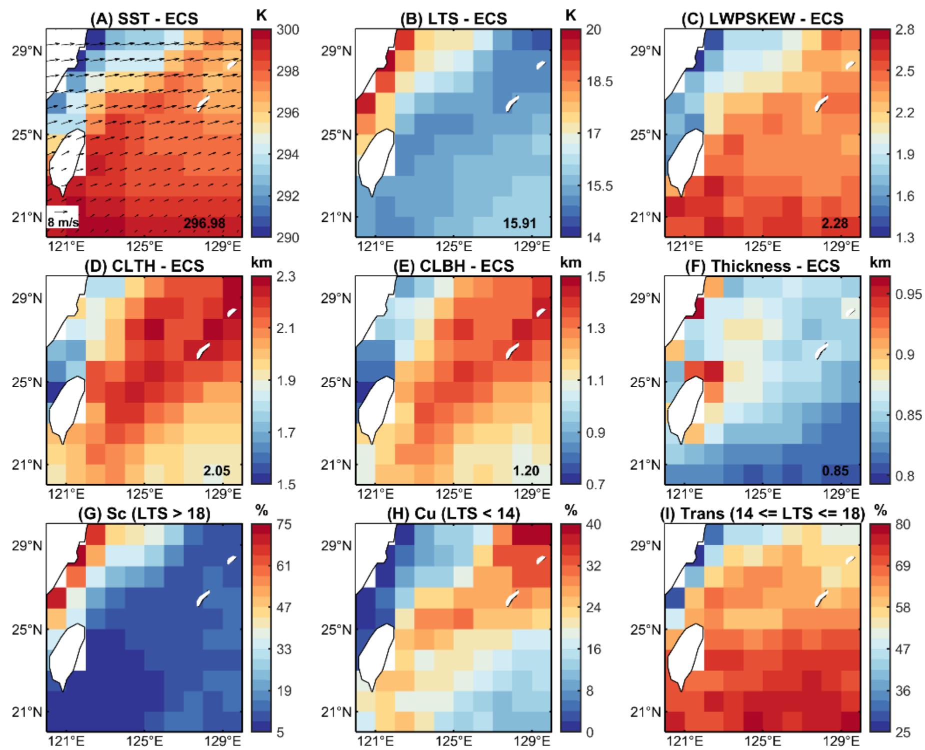

~~**Figure 4. Distributions of meteorological factors and different cloud regimes in ECS region.** (A) Sea Surface Temperature (SST), the composite wind field (arrows) on 700 hPa and (B) lower-tropospheric stability (LTS) are from ERA5 reanalysis data. (C) LWP skewness, (D) cloud-top height (CLTH), (E) cloud base height (CLBH) and (F) cloud thickness are directly or indirectly derived from SatCORPS Himawari-8 product. The numbers in the lower right corner represent regional averages being weighted by the cosine of latitude. Distribution of the proportion of cloud regimes for (G) Stratocumulus (Sc, LTS > 18 K), (H) Cumulus (Cu, LTS < 14 K), (I) Sc to Cu transition regime (Trans, 14 K <= LTS <= 18 K).~~

~~Finally, at high aerosol-loading conditions, warm invigoration has been found in numerous studies. For instance, Kaufman et al. (2005) reported larger LWP in higher aerosol loading conditions over Atlantic warm clouds (a mix of stratus and trade cumulus) using MODIS observations. Yuan et al. (2011) found increased cloud amount and higher cloud top heights associated with volcanic aerosols in trade cumulus near Hawaii with A-Train satellites. In contrast to the model results of Koren et al. (2014), who suggested that warm invigoration saturates at higher aerosol loading (AOD ~ 0.3), our findings indicate a higher AOD of 0.41 (Figure 2), which is reasonable because the saturation value of AOD exhibits regional variability. For example, Kaufman et al. (2005) reported a maximum AOD of 0.46, while Zhang et al. (2021) found that the AOD in the ECS region is approximately 0.4. To summarize, these evidences all confirm the plausibility of warm invigoration in the ECS region, causing the positive LWP adjustments at high N_d.~~

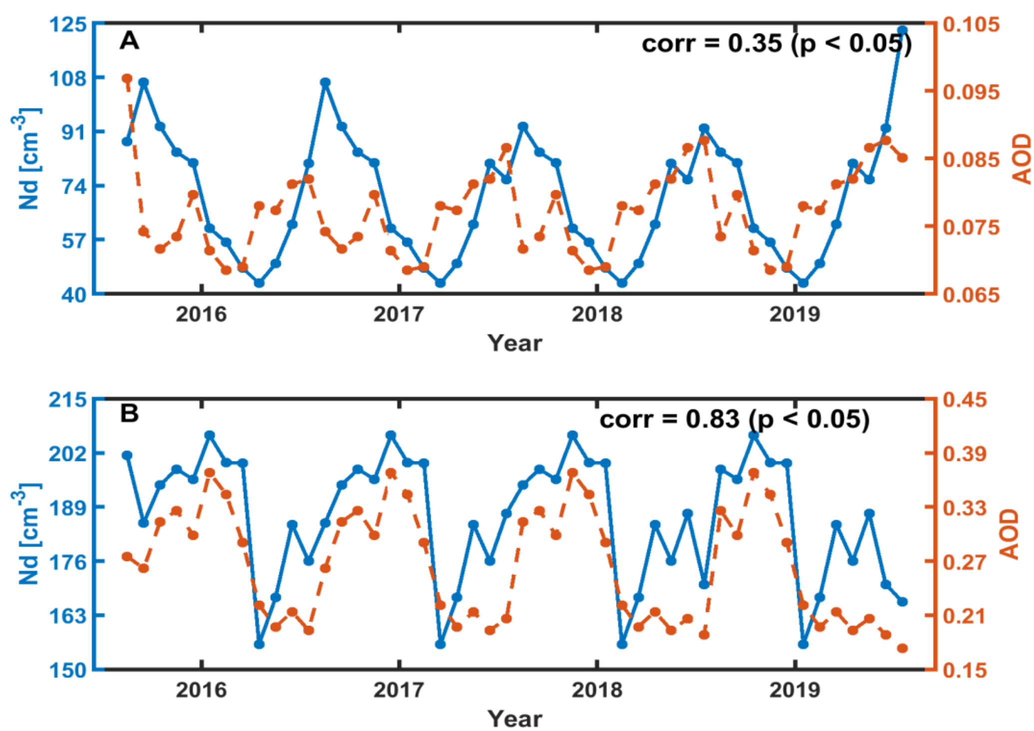

~~**Figure 5. 4-year long-term variations of N_d and total aerosol optical depth (AOD) from MERRA-2 at 1200 LT in AUW (A) and ECS (B) region.** The correlation coefficients (corr) between N_d and AOD are 0.35 and 0.83 (significant at the 95% confidence level), respectively.~~

~~Note that we select the column AOD as an aerosol proxy to remain consistent with the above studies. Although AOD may not represent aerosol concentrations in some conditions, Figure 5 shows significant correlations observed between the 4-year long-term variations of AOD and N_d at 1200 LT in both regions, particularly in ECS with a correlation of 0.81. Meanwhile, both regions show the similar distribution patterns, with higher N_d and smaller r_e near the continental coastal area, aligning~~

~~with the average AOD spatial distribution (spatial correlation coefficients of 0.84 in AUW and 0.91 in ECS) (Figure S1), suggesting the availability of AOD as an aerosol proxy.~~

~~Furthermore, a sensitivity analysis is conducted to exclude the influence of Simpson's Paradox. Due to thicker cloud samples along the coast with larger N_d and thinner ones with smaller N_d offshore in ECS region, we divide the samples into coastal and offshore groups and find that the observed pattern is not significantly affected by the geographical region (Figure S3). Considering the different processes associated with cloud regimes, we conducted a similar analysis for each cloud regime. Our findings reveal that the pattern of LWP adjustments is insensitive to cloud regime (Figures S4-S6), suggesting that they can be studied collectively.~~

~~We further analyze the influence of meteorological conditions (i.e., LTS and RH) on LWP adjustments in the two regions (Figure S7). Overall, LWP adjustments cannot be explained by a single meteorological factor. For example, in ECS region, despite the similarity in diurnal patterns of LWP adjustment within different LTS bins, the magnitudes exhibit significant differences due to different aerosol loadings. Samples with LTS > 18 K are concentrated in coastal areas with higher aerosol loadings. Warm invigoration is stronger for these samples, thus the overall LWP adjustment is positive. In contrast, samples with LTS < 18 K have a larger proportion of smaller aerosol loadings. The effect of entrainment feedback is more pronounced. This further highlights the importance of aerosol loadings in regulating LWP adjustments in ECS region. Meanwhile, the intricate interplay among meteorological factors, clouds, and aerosols makes it difficult to exclude the influences from meteorological factors (Chen et al., 2014; Engström and Ekman, 2010; Zhang and Feingold, 2023).~~

are presented in Fig. S2. The N_d-LWP relationships show similar patterns during daytime in each region, but different results in the two regions. The overall LWP adjustments are –0.31 in the AUW and 0.02 in the ECS region. For N_d < ~300 cm^{-3}, LWP decreases with increased N_d, which is typically attributed to sedimentation-entrainment feedback (Ackerman et al., 2004) and evaporation-entrainment feedback (Small et al., 2009), leading to negative LWP adjustments in both regions. However, LWP begins to rise at high N_d (> ~300 cm^{-3}), exhibiting an overall V shape, particularly in the ECS region, where clouds are downwind of the major emission sources of China. 18% of the samples in the ECS region exhibited N_d values exceeding 300 cm^{-3}. To investigate whether the positive N_d-LWP relationship is influenced by broken scenes, we assessed the sensitivity of our results to CF. As shown in Fig. S3, the rise in LWP at high N_d coincides with an increase in CF. The average CF for samples with N_d > 300 cm^{-3} is 86%. Additionally, the positive N_d-LWP relationship persists in both overcast (CF > 80%) and broken (CF < 80%) cloud scenes. This consistency indicates that the observed LWP increase at high N_d is unlikely to be an artifact of broken-cloud scenes.

The V shape observed in our results differs from the inverted-V shape reported in previous studies (Glassmeier et al., 2021; Gryspeerdt et al., 2019). Specifically, it is characterized by the absence of an ascending branch at low N_d and the emergence of an ascending branch at high N_d. The inverted-V shape is typically associated with positive LWP adjustments at low N_d, which have been linked to precipitation suppression (Albrecht et al., 1995). That is, as increasing N_d, the reduced r_e may enhance the stability against coalescence and suppress the precipitation and loss of LWP (Albrecht, 1989; Glassmeier et al., 2021). The positive slopes are often observed in very pristine environments (Gryspeerdt et al., 2023), especially when N_d

is below approximately 10 cm^{-3} (Fons et al., 2023; Goren et al., 2025). In contrast, in this study, 98% of the AUW samples exhibit N_d values exceeding 15 cm^{-3}, and 99% of the ECS samples have N_d greater than 30 cm^{-3}. Therefore, we did not find this positive slope of the inverted-V shape. Nevertheless, the LWP increasing signal resulting from precipitation suppression is still detectable in our study. For instance, samples with $r_e > 14$ µm—conditions more likely to contain drizzle (Rosenfeld et al., 2012)—still exhibit a weaker negative LWP adjustment than those with $r_e < 14$ µm (Fig. 1, –0.22 vs. –0.47 in the AUW and -0.13 vs. -0.23 in the ECS), consistent with the results of Zhou and Feingold (2023) in the northwestern Atlantic. It suggests that in drizzle-like samples, the precipitation suppression partially offsets the dominant LWP reduction caused by the entrainment effect, resulting in a weak decrease in LWP with increasing N_d compared to non-drizzle samples.

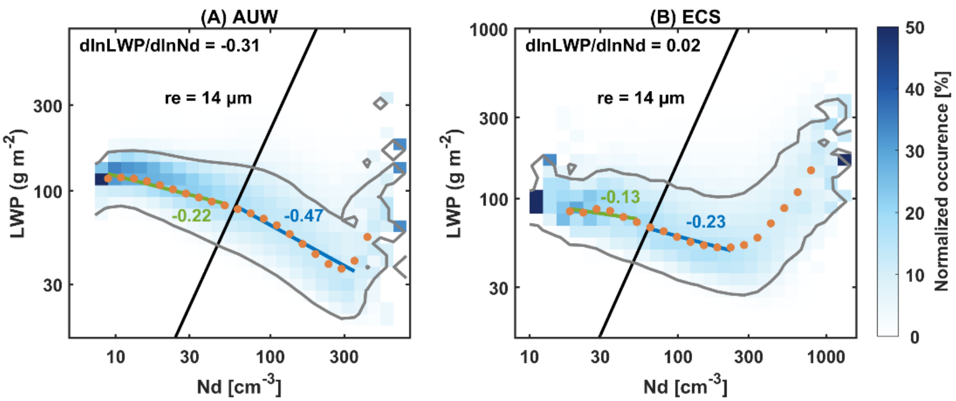

Figure 1: Joint histograms of N_d and LWP in log-log space in the AUW and ECS regions. The column of each N_d bin is normalized. The black lines are fitted based on the bins in the joint histogram with the effective radius (r_e) closest to 14 µm. The gray lines represent the contour of 5% occurrence. Orange dots represent the median LWP in each N_d bins with a sample size greater than 50. The green and blue lines are regression slopes for the orange points with r_e above and below 14 µm, respectively.

In this study, the ascending branch of the V shape at high N_d condition (> ~300 cm^{-3}) is the main reason for the overall positive LWP adjustments in the ECS region. Positive sensitivity of LWP to N_d perturbations over the ECS has been reported but not fully understood (Bender et al., 2019; Gryspeerdt et al., 2019; Michibata et al., 2016; Zhang et al., 2021). Here, our results indicate a strong transition in meteorological conditions across the turning point of V shape (Fig. 2), suggesting large-scale meteorology as a possible driver.

Meteorological conditions significantly modulate cloud microphysical processes (e.g., cloud droplet activation, condensation, entrainment, collision-coalescence, and precipitation) (Feingold et al., 2025), which in turn alter both the sign and magnitude of LWP adjustments, particularly within the sharp environmental transition from coastal to offshore areas in the ECS region. Kuroshio Current produces a sharp SST gradient in the ECS region (shown in Fig. S4A), leading to a distinct transition in boundary layer thermodynamic structure and cloud properties from the coast to offshore areas (Liu et al., 2016).

Following Rosenfeld et al. (2019), we categorize the clouds into three regimes, i.e., Sc (LTS > 18 K), Sc to Cu transition (14 K ≤ LTS ≤ 18 K), and Cu (LTS < 14 K) (Fig. S4, B, C, and D). Sc presents over a cooler sea surface along the coast (Fig. S4, A and B). The coastal distribution suggests that most of Sc may be advected from the Sc region in the southeast Chinese plain (Klein and Hartmann, 1993). According to the cloud advection scheme by Miller et al. (2018), cloud advection can be approximated as a translation of the cloud field with the wind field. The advection height is assumed to correspond to the height of the cloud top. Based on the 700 hPa wind field (Fig. S4A), it is plausible that Sc in the ECS region is possibly advected from the southeast Chinese plain. As air moves offshore, the cloud layer decouples with the surface mixed layer over the warmer sea surface—a process known as the "deepening-warming mechanism" (Albrecht et al., 1995). In this decoupled boundary layer, Cu forms in the moist and unstable subcloud layer and rises to the upper cloud layer, resulting in a locally cumulus-coupled MBL.

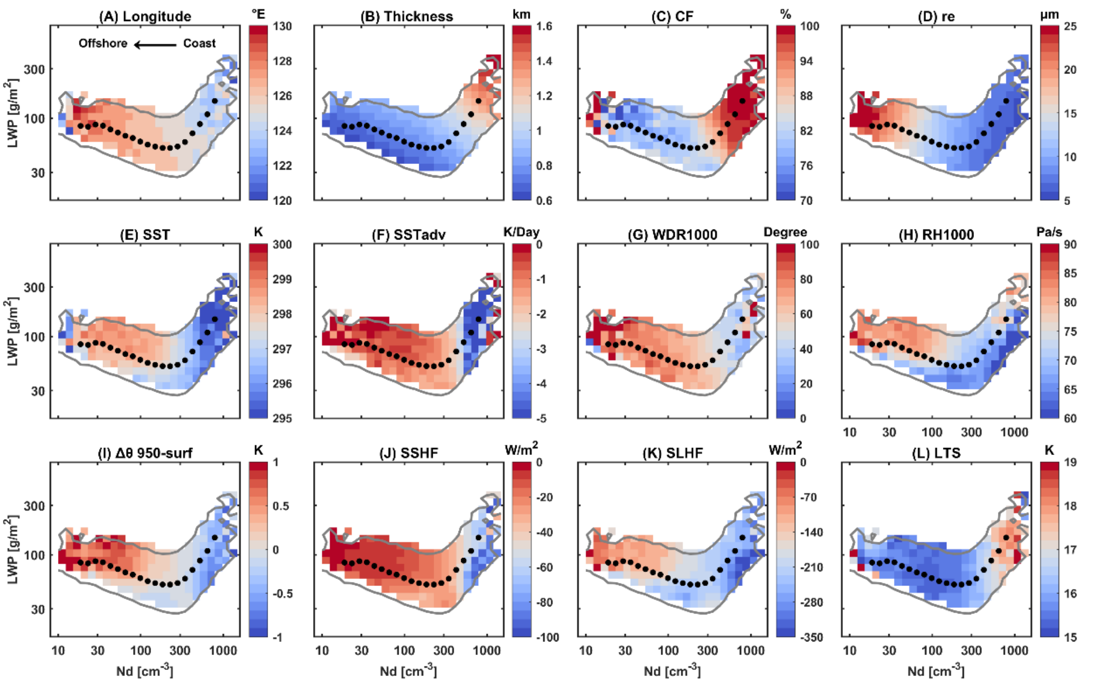

Figure 2: Distributions of meteorological conditions in N_d-LWP log-log space in the ECS region. The color scale represents the median values in each bin. Only bins with an occurrence of at least 5% are shown, bounded by the gray lines. (A) Longitude. (B) Cloud thickness. (C) Cloud fraction (CF). (D) Cloud effective radius (r_e). (E) Sea surface temperature (SST). (F) Horizontal temperature advection at the surface (SST_{adv}). (G) Wind direction on 1000 hPa. 0° indicates a northerly wind. (H) Relative humidity on 1000 hPa (RH1000). (I) The potential temperature difference between 950 hPa and 2 m above the sea surface ($\Delta\theta_{950\text{-surf}}$), a proxy of the sub-cloud layer stability. (J) Surface sensible heat flux (SSHF). (K) Surface latent heat flux (SLHF). For the vertical fluxes, the negative is upwards. (L) Lower-tropospheric stability (LTS). Black dots represent the median LWP in each N_d bins with a sample size greater than 50.

The cloud samples in the ascending branch are concentrated west of 125°E and dominated by continental air masses (Fig. 2A), which are characterized by strong northerly cold air advection at the surface that destabilizes the air-sea interface (Fig. 2, F and G). The potential temperature difference between 950 hPa and 2 m above the sea surface ($\Delta\theta_{950\text{-surf}}$) is calculated as an indicator of sub-cloud layer stability, revealing an extremely unstable sub-cloud layer in the ascending branch (Fig. 2I). Northerly winds transport relatively dry, cold, aerosol-rich air across the warm ocean (Fig. 2, F, G, and H). This destabilizes the sub-cloud layer and intensifies the upward fluxes of sensible and latent heat from sea surface into the atmosphere (Fig. 2, I, J and K) (Long et al., 2020), raising saturation water vapor pressure and facilitating cloud droplet activation. Additionally, high LTS along the coast (Fig. 2L) suppresses vertical mixing at cloud top (Scott et al., 2020), allowing activated droplets to accumulate more liquid water with thicker clouds (Fig. 2B) and higher CF (Fig. 2C). These conditions jointly elevate both N_d and LWP, forming the ascending branch of the V shape pattern.

While cold air outbreaks (CAOs) also contribute to the observed increases in both N_d and LWP, our analysis suggests that cold air advection is a more consistent and seasonally pervasive driver and CAOs represent a strong form of cold air advection. Following Papritz et al. (2015), the Cold Air Outbreak Index (CAOI) was calculated as the difference in potential temperature between the surface skin and 850 hPa. CAO events are identified when CAOI > 0. Our results indicate that CAOs are most pronounced in autumn and winter, with no significant occurrence in spring (Fig. S5). Results of summer are statistically insignificant due to the limited samples (3%), particularly after excluding cases with strong precipitation (GPM = 0 mm hr^{-1}). The seasonal variations are consistent with the East Asian monsoon, where strong northerly winds prevail in winter but weaken in spring (Liu et al., 2016), leading to reduced CAOI. In contrast, the impacts of cold air advection are prevalent throughout the seasons (Fig. S6), making it a more plausible reason for the observed sub-cloud destabilization and subsequent increases in N_d and LWP.

In the AUW region, LWP also increases when N_d exceeds 300 cm^{-3}. However, the region is relatively clean with only 0.02% of all samples exhibiting N_d above ~300 cm^{-3}. Given the limited sample size, these results are not statistically representative, and only a brief discussion is provided here. Samples with N_d > ~300 cm^{-3} still demonstrate distinct meteorological conditions compared to samples with N_d < ~300 cm^{-3} (Fig. S7). In contrast to the ECS region, pollution sources in the AUW region originate from lower latitudes (Fig. S7A). This may be attributed to the influence of warm and moist environment over the warm ocean with weak large-scale subsidence (Fig. S7, E, H, and L), which promote cloud droplet activation and consequently lead to positive LWP adjustments at high N_d.

The above results suggest that the impact of large-scale meteorology on cloud microphysical processes ultimately determines the pattern of LWP adjustment. Previous studies employed various methods to exclude environmental confounding factors, such as opportunistic experiments from ship-track or volcano eruptions (Chen et al., 2022; Toll et al., 2019), where an overall weak LWP adjustment was observed. For satellite studies, ~~Rosenfeld et al. (2019)~~Rosenfeld et al. (2019) pointed out that cloud thickness (H) ~~explained almost three-fourths~~constrained most of the meteorological impacts~~ on cloud radiative effect (CRE)~~, and ~~they~~N_d explained nearly half of the LWP variability for a given H. They demonstrated an overall positive LWP adjustment when separating H. However, we find that LWP adjustments become negative after constraining H in the intervals of ~~Figure~~Fig. ~~1~~3 (B and E), indicating the dominant effect of entrainment ~~processes~~ feedbacks. The discrepancy may arise from their focus on samples in convective cores (top 10% of cloud optical thickness), which are closer to adiabatic, whereas our samples suggest more exchange with the free atmosphere.

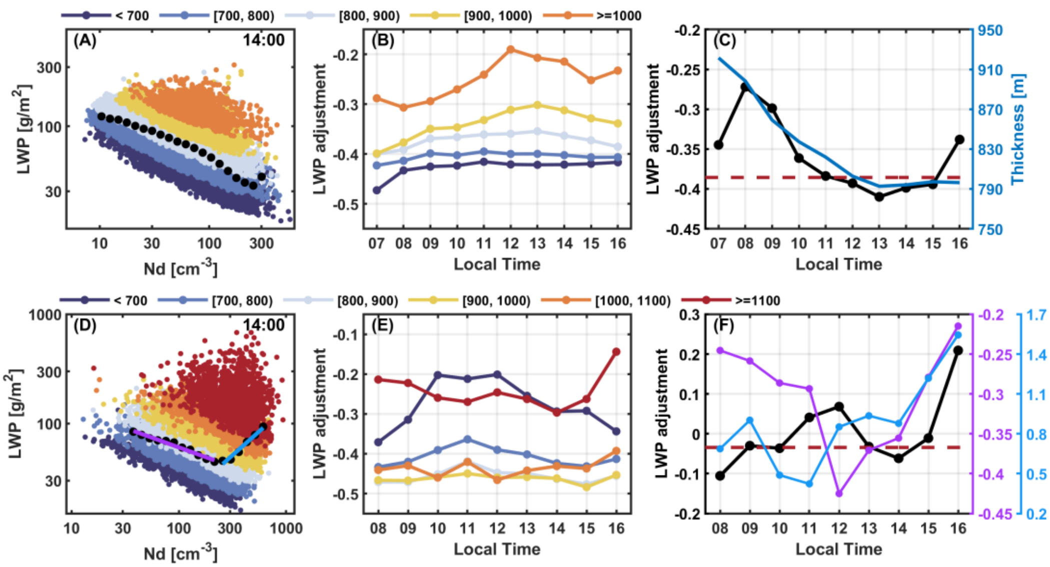

Figure 3: LWP adjustments in log-log spaces and their diurnal patterns in two typical regions (the west of Australia, AUW and the East China Sea, ECS). Cloud samples are scattered in N_d-LWP log space at 1400 LT in the (A) AUW and (D) ECS region. The complete pictures of all available daytime are presented in Fig. S11. Colored dots are samples in different cloud thickness (H) bins (unit: m). Black dots represent the median LWP in each N_d bin. The colored lines are the fits of black dots at different stages in the ECS region. Diurnal variations of LWP adjustments binned by H in the (B) AUW and (E) ECS regions are shown. Colored lines in (F) are diurnal variations of different stages in (D), while black lines in (C) and (F) are the overall diurnal variations of LWP adjustments in two regions, respectively. The blue line in (C) represents the diurnal variation of H. ~~Fons et al. (2023) suggested H is an important confounder using a causal approach and should be conditioned on.~~ Red dashed lines represent the average LWP adjustments during MODIS Terra (1030 LT) and Aqua (1330 LT) overpasses, –0.39 for the AUW region (C) and –0.03 for the ECS region (F).

Here, our results indicate the physical significance of constraining H. ~~The sensitivity of LWP adjustments to H is observed in Figure 1. In~~In the AUW region, negative LWP adjustments become weaker as H increases~~.~~ (Fig. 3B). H alters LWP adjustments by influencing cloud microphysical processes, such as promoting condensation growth (Fons et al., 2023). Thicker clouds with higher cloud-top r_e are less sensitive to entrainment-feedbacks with increasing N_d compared to thinner clouds ~~(Figure 1B).~~. In other words, LWP in different H intervals responds differently to N_d, so it is necessary to restrict H to exclude the effects of ~~covariation~~covariations. However, in the ECS region, negative LWP adjustments for clouds with H < 900 m become stronger with increasing H, while for clouds with H > 900 m, quite the contrary: it weakens with increasing H~~.~~ (Fig. 3E). The bidirectional sensitivity of LWP adjustments to H is likely attributed to distinct mixing characteristics among different cloud regimes in ~~ECS region, reflecting the complex interactions between meteorological factors, clouds, and aerosols. Additionally, clouds above 800m are associated with warm invigoration (Figure 2D). In this condition, H serves as a mediator but not a confounder. This implies that constraints on H in ECS is inappropriate because they fundamentally restrict~~the ECS region. Constraining H in the ECS region restricts a majority of mechanisms influencing cloud vertical development. Cloud thickness typically serves as a mediator for large-scale meteorology (such as cold air advection, LTS, and surface heat fluxes) to influence LWP. These processes are particularly evident in the ECS region, where the increase in LWP at high N_d corresponds with an increase in cloud thickness (Fig. 2B). Therefore, the stratification of cloud thickness can isolate a significant portion of covariations, highlighting the impact of N_d on LWP.

In summary, the above results ~~indicate~~reveal that LWP adjustments strongly depend on microphysical-dynamical processes (e.g., precipitation suppression, and entrainment feedbacks~~ with increasing N_d~~) and large-scale meteorology (e.g., cold air advection and the stability of MBL). Given that some of these factors display diurnal variations in ~~AUW region. While in ECS region~~response to the solar radiation cycle, LWP adjustments ~~are results of the competition between entrainment feedbacks and warm invigoration. Given that LWP adjustment is influenced by a complex interaction of meteorological factors, we think~~would also exhibit diurnal patterns (black lines in Fig. 3, C and F). We surmise that ~~cloud~~the prevailing dynamic conditions ~~provide more reliable indications. Specifically, cloud thickness is important in AUW region, whereas aerosol loading (represented by N_d) is a better indicator in the ECS region. Therefore, the diurnal variations of these factors can provide important indications~~at any given time are responsible for ~~us to investigate~~ the ~~potential mechanisms driving~~observed diurnal variations of LWP adjustments. To verify this hypothesis, we investigated the diurnal variations in LWP adjustments and their potential influencing factors.

3.2 How LWP adjustments change over the diurnal scale and associated mechanisms

~~In~~LWP adjustments exhibit pronounced diurnal variations with distinct regional contrasts. In the AUW region, the negative LWP adjustments strengthen from around 0800 LT to 1300 LT, reaching ~~the~~their strongest value at –0.41, and then ~~weakening~~weaken to –0.34 (black line in ~~Figure~~Fig. ~~1C~~3C). In the ECS region, the positive LWP adjustments exhibit two local peaks during the observation period, occurring at 1200 LT and 1600 LT, with peak values of 0.07 and 0.21, respectively (black line in ~~Figure~~Fig. ~~1F~~3F). And two local minima LWP adjustments are observed at 0800 LT and 1400 LT, with values of –0.11 and –0.06, respectively. ~~Meteorological conditions have a small impact on the diurnal patterns of LWP adjustments in both regions (Figure S7).~~The results highlight the limitations of using the sparse polar-orbiting satellite observations to represent LWP adjustment at specific times. For example, MODIS overpass averages (red dashed line in Fig. 3C) overestimate the intensity of negative LWP adjustment in the AUW region by 44% at 0800 LT. In the ECS region, the intensity of negative LWP adjustments are underestimated by 73% at 0800 LT, while the intensity of positive adjustments at 1600 LT are underestimated by 114% (Fig. 3F). Such biases can lead to substantial errors in estimation of ACI (see Section 4 for details).

We first analyze the role of meteorological factors in driving the diurnal variations of LWP adjustments (Fig. S8). Overall, the covariance of a single meteorological factor affects only the magnitude of LWP adjustments. In the AUW region, the lower LTS corresponds to weaker negative LWP adjustments. Samples with relatively low LTS are characterized by larger r_e in the N_d-LWP space (Fig. S9), leading to stronger precipitation suppression by increasing N_d and thus a weaker negative LWP adjustment. In the ECS region, stronger cold air advection corresponds to greater sensible and latent heat fluxes, resulting in more positive LWP adjustments, which is consistent with the findings presented in the previous section. The diurnal variations of LWP adjustments cannot be explained by a single meteorological factor. Therefore, it is necessary to start with the diurnal variations of cloud properties to analyze the mechanisms behind the diurnal LWP adjustment patterns~~ of LWP adjustments~~.

The AUW region is one of the subtropical Sc regions over the eastern part of the ocean away from continents (Klein and Hartmann, 1993), characterized by large LTS and strong large-scale subsidence (~~Figure~~Fig. ~~3~~S10), which are favorable for the formation of Sc. Figure ~~6~~4 depicts the diurnal variations of cloud properties in the Sc-like AUW region. The diurnal variation of LWP shows a typical pattern with a peak in the morning and a gradual reduction until early afternoon. According to previous studies, this pattern is subject to the diurnal cycle of solar insolation (Bretherton et al., 2004; Mechoso et al., 2014; Wood et al., 2002). Specifically, during the daytime, solar radiation absorption within the cloud layer and long-wave cooling at the cloud top drive the turbulent mixing within the cloud layer and inhibit turbulence to the sea surface, thus leading to the decoupling of the cloud-topped marine boundary layer (MBL) ~~(Duynkerke and Hignett, 1993; Ghosh et al., 2005; Slingo et al., 1982)~~(Duynkerke and Hignett, 1993; Ghosh et al., 2005; Slingo et al., 1982). As decoupling cuts off the moisture source from the sea surface, the imbalance between entrainment drying and upward moisture flux may thin the cloud layer. The decrease of LWP before 1300 LT is primarily attributed to the lifting of the cloud base, indicating that entrainment drying originates from evaporation at the cloud base, which is in line with an early modeling study for typical Sc cloud regimes (Bougeault, 1985). After 1300 LT, the gradual reduction of solar heating hinders the intensification of decoupling and helps rebuild the turbulence between the cloud and subcloud layer. Therefore, LWP increases after 1300 LT likely due to the reconstruction of turbulence.

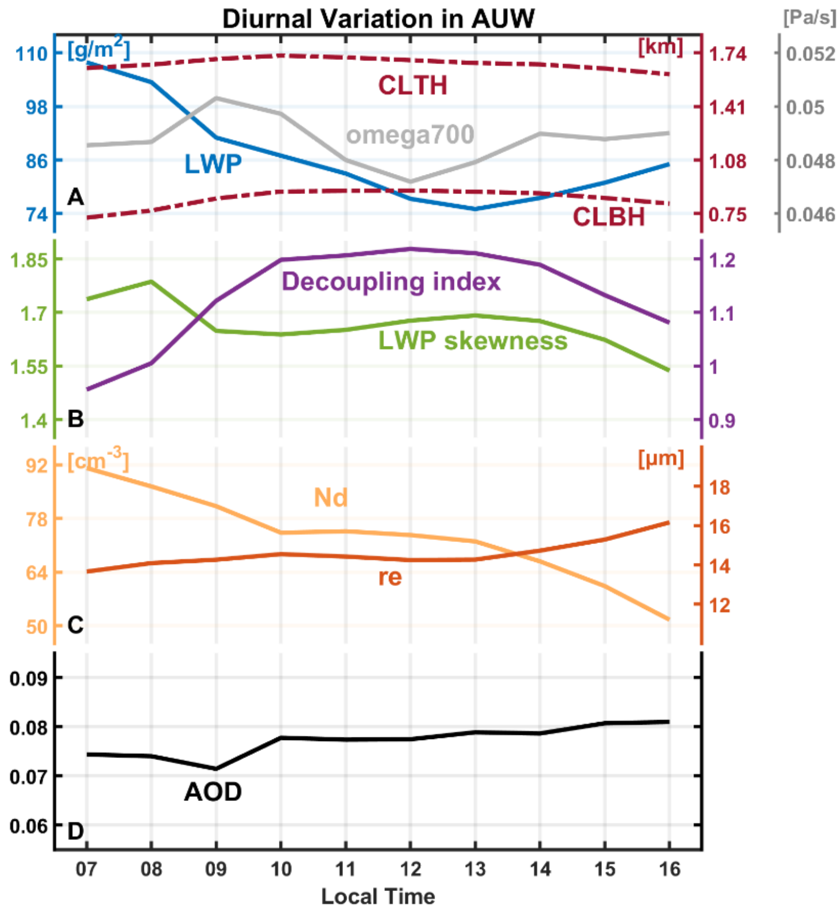

Figure ~~6~~4:~~.~~ Diurnal patterns in the AUW region. (A) Cloud liquid water path (LWP), cloud-top height (CLTH), cloud base height (CLBH~~)~~), and vertical velocity on 700 hPa (omega700, positive values indicate downdraft) from ERA5 reanalysis. (B) LWP skewness and decoupling index in the AUW region. (C) Cloud droplet number concentration (N_d) and effective radius (r_e). (D) Aerosol optical depth (AOD).

Following the quantification method of Zheng et al. (2018) and Kazil et al. (2017), this study presents auxiliary verifications of the decoupling process. First, according to Zheng et al. (2018), decoupling of the subtropical Sc decks during cold advection is often unstable (negative temperature advection). The formation of Cu beneath the Sc will render local coupling by feeding moisture into the upper cloud layer, thus causing a positive skewness of the probability density function (PDF) of LWP. Therefore, the skewness of the LWP PDF can be used to estimate the degree of decoupling for each cloud sample:

$$\text{skewness} = \frac{E(x-u)^3}{\sigma^3} \tag{3}$$

where E is the expected value, μ and σ is the mean and standard deviation of x, respectively. Positive skewness indicates more data tends to be distributed to the right, and vice versa. Larger LWP skewness indicates a larger decoupling degree.

As shown in ~~Figure~~Fig. ~~6~~4, LWP skewness increases before 1300 LT and then decreases, illustrating the decoupling process discussed above. Note that while the cumulus penetration alters LWP, small variations in LWP skewness suggest that it cannot be directly compared with the reduction of LWP caused by decoupling, thus having no evident effect on the diurnal variation of LWP over the AUW region. Additionally, due to the fluctuation of LWP skewness before 0900 LT, another decoupling index defined by Kazil et al. (2017) is used for further indication, quantifying the relative position between the CLBH and the lifting condensation level (LCL). A larger index implies a stronger degree of decoupling:

$$\text{decoupling index} = \frac{CLBH - LCL}{LCL} \tag{4}$$

LCL is derived from ERA5 reanalysis following Wood and Bretherton (2006). The two ~~indexes~~indices support each other and confirm the decoupling process.

~~Unexpectedly, there is no evident diurnal variation of AOD in AUW, but~~ N_d continually declines from 0700 LT to 1600 LT and r_e does not change significantly before 1200 LT and then rises. ~~It~~In contrast, there is ~~thus~~no evident diurnal variation of AOD in the AUW, which is reasonable in the remote ocean area but insufficient to ~~infer~~explain the diurnal variations of N_d and r_e ~~are related with dynamic process on account of the disagreement with~~. This suggests that other factors rather than aerosols may be responsible for the diurnal variations~~. Combing~~ of N_d and r_e over the AUW region. Combining the nature of the decoupling process and diurnal patterns of cloud properties in ~~Figure~~Fig. ~~6~~4, we discuss the possible mechanisms for the diurnal variation of N_d and r_e based on earlier cloud microphysics studies. According to Verlinden (2018), the shortwave heating counteracts longwave cooling during daytime, resulting in weakening of cloud-top entrainment. Meanwhile, the decoupling that cuts off moisture transport suppresses condensational growth. The combination of these two processes may lead to ~~the~~ little ~~variation~~variations in r_e before 1200 LT. Additionally, the decoupling process leads to the suppression of both surface moisture transport and cloud base updrafts, which may in turn reduce the supersaturation and hence the number of activated cloud droplets. This may explain the continuous decrease in N_d before 1300 LT. Furthermore, according to the relationship between CLTH, w_s (always negative~~)~~)), and entrainment rate (w_e) ($\frac{dCLTH}{dt} = w_s + w_e$) in the mixed-layer model framework (Painemal et al., 2013), we explain the variations after 1200 LT. CLTH begins to decrease after 1200 LT, suggesting an intensification of large-scale subsidence (w_s, always negative in Sc region) and/or a weakening of entrainment rate (w_e). Large-scale subsidence on 700 hPa from ERA5 reanalysis becomes stronger (gray line in ~~Figure~~Fig. ~~6A~~4A). It may enhance the temperature-inversion jump, which will in turn decrease the entrainment rate (Painemal et al., 2013). During this period, the condensational growth by the reconstructed water vapor supply will enhance r_e. Meanwhile, the coalescence process, enhanced by an increase in r_e leads to a decrease in N_d. This process could be more dominant than the increase in activated cloud droplets caused by water vapor reestablishment for an increase in N_d to be observed in this study.

Based on the diurnal mechanisms of MBL discussed above, the diurnal LWP adjustment pattern~~ of LWP adjustments~~ is primarily a consequence of the influence of these diurnal-related mechanisms on the relationship between N_d and LWP~~ across different microphysical-dynamical conditions.~~. In the AUW region, the diurnal variations of the overall LWP adjustments (black line in ~~Figure~~Fig. ~~1C~~3C) and cloud thickness (blue line in ~~Figure~~Fig. ~~1C~~3C) demonstrate a strong consistency with a turning point at 1300 LT. The variation of LWP adjustment here is mainly attributed to the gradual thinning of clouds, which reflects the differential LWP responses to N_d with varying H. LWP adjustment becomes more negative with the thinning of ~~cloud~~clouds, which is consistent with the results in ~~Figure~~Fig. ~~1B~~3B. After 1300 LT, cloud thickness remains almost unchanged. The variation in LWP adjustments is mainly governed by the weakening of entrainment due to the intensification of large-scale subsidence (~~Figure~~Fig. ~~6A~~4A). During this time, the weakening of the entrainment process leads to a weakening of the negative LWP adjustments over the AUW region.

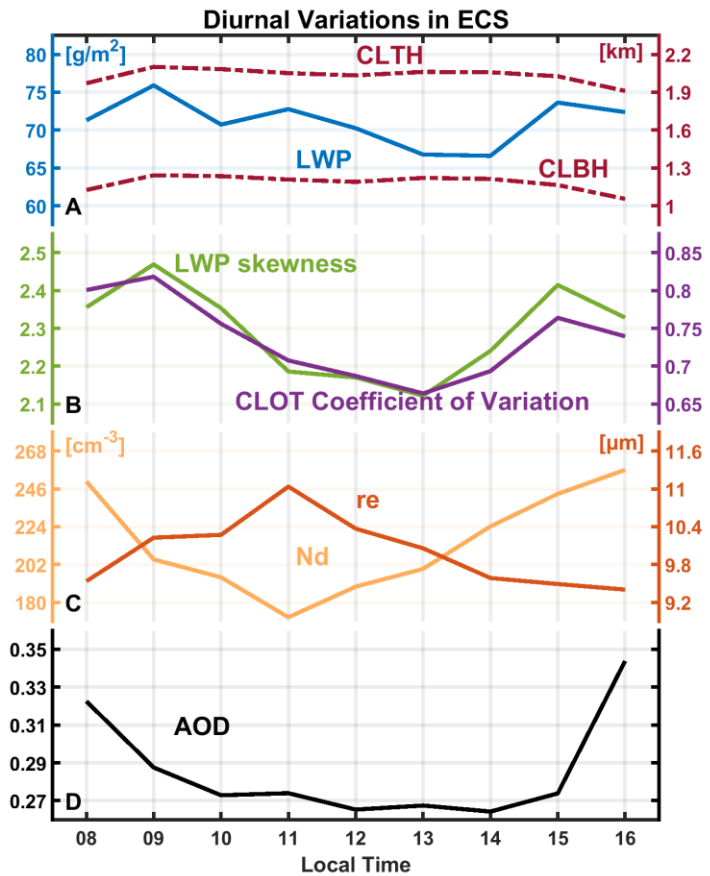

~~**Figure 7. Diurnal patterns in ECS region.** (A) Cloud liquid water path (LWP), cloud-top height (CLTH) and cloud base height (CLBH). (B) LWP skewness and coefficient of variation (c_v) of cloud optical depth (CLOT) in AUW region. (C) Cloud droplet number concentration (N_d) and effective radius (r_e). (D) Aerosol optical depth (AOD).~~

In contrast, conditions ~~in~~of MBL in the ECS region are more complicated. As mentioned in the last section, the ECS is a Sc-Cu transition region due to the "deepening-warming" process. Under this condition, MBL is seldom fully ~~coupled~~decoupled but exhibits local cumulus coupling. Apparently, LWP skewness is a more appropriate indicator to reflect cumulus coupling in this region. ~~Furthermore, the spatial distribution of LWP skewness can indicate the influence of cumulus coupling offshore (Figure 4C).~~ For diurnal variations in the ECS in ~~Figure~~Fig. ~~7~~5, there is a general decrease in LWP before 1300 LT, followed by an increase. This is in contrast to the pronounced cloud thinning observed in the AUW region due to the decoupling of MBL by solar heating. In the ECS region, the overall change of LWP is not significant (less than 10 g/m^2). Since MBL is never fully coupled, these minor observed changes are mainly caused by local cumulus coupling. The variations of LWP and LWP skewness exhibit a strong consistency. We also calculate the coefficient of variation (c_v) of CLOT to represent the uniformity of each cloud sample. c_v is defined as the standard deviation (σ) divided by the mean(μ):

$$c_v = \frac{\sigma}{\mu} \tag{5}$$

The smaller the c_v is, the less dispersion there is among the cloud pixels in the cloud sample, resulting in a more uniform sample. It turns out that the cloud layer is influenced primarily by the strength of cumulus coupling, rather than other factors.

In the ECS region, the weakest cumulus activity occurs at 1300 LT (the lowest LWP skewness in ~~Figure~~Fig. ~~7B~~5B), which may be attributed to solar insolation. In the Sc to Cu transition region, the decoupled cloud layer and subcloud layer are often separated by a stable transition layer, which has been widely observed by the Atlantic Stratocumulus Transition Experiment (ASTEX) conducted over the northeast Atlantic Ocean. Based on ASTEX, Rogers et al. (1995) suggested that the shortwave radiation would hinder convection during daytime by increasing the stability of the transition layer. Miller et al. (1998) extended this theory to the diurnal variations and believed that the diurnal variation of Cu development was regulated by the stability of the transition layer.

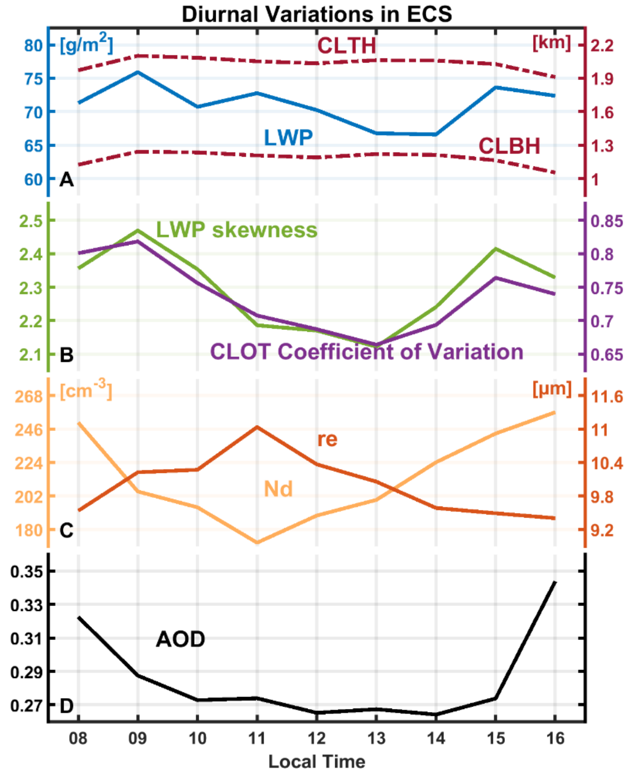

Figure 5: Diurnal patterns in the ECS region. (A) Cloud liquid water path (LWP), cloud-top height (CLTH) and cloud base height (CLBH). (B) LWP skewness and coefficient of variation (c_v) of cloud optical depth (CLOT) in the AUW region. (C) Cloud droplet number concentration (N_d) and effective radius (r_e). (D) Aerosol optical depth (AOD).

In terms of microphysical properties, N_d in the ECS decreases before 1100 LT and then increases. Variations of r_e are just the opposite except insignificant change since 1400 LT. The crucial mechanism leading to such changes may be attributed to the weakest entrainment drying at 1100 LT, resulting in the highest values of r_e and the lowest values of N_d. Such diurnal variations in entrainment have also been observed in other coastal areas. Caldwell et al. (2005) reported the weakest entrainment rate at 1100 LT during the East Pacific Investigation of Climate (EPIC) stratocumulus cruise in 2001. ~~Painemal et al. (2017)~~Painemal et al. (2017) found the minimum of entrainment occurred between 0900-1100 LT over the northeast Pacific region, attributing the diurnal pattern to the turbulence caused by long-wave radiative cooling. Additionally, other factors may also contribute to the diurnal variations of N_d and r_e. For example, the changes before 1100 LT may include the impacts of reducing aerosol loadings. Subsidence from both cloud top and bottom occurred after 1400 LT may limit the entrainment and the continuous decline of r_e. Cumulus coupling may also contribute to the increase of N_d, and Martin et al. (1995) found a local increase in N_d induced by the intrusion of cumulus clouds during ASTEX.

~~In ECS region, based~~Based on the above mechanisms, the diurnal variation of LWP in the ECS region is relatively small, yet N_d exhibits a distinct diurnal pattern. Changes in N_d ~~lead to~~determine the slope of LWP adjustments at the ascending and descending branches of the V shape that correspond to ~~two microphysical-dynamical processes. The~~different meteorological conditions. The N_d turning point between the two stages exhibits the same diurnal variation as the average N_d (~~Figure~~Fig. ~~S8~~S12). Before noon, a decrease in N_d weakens the ~~warm invigoration~~positive branch (blue line in ~~Figure~~Fig. ~~1F~~3F), while the ~~entrainment feedback~~negative branch intensifies (purple line in ~~Figure~~Fig. ~~1F). After 1200 LT, the trend reverses. The opposing patterns between warm invigoration and entrainment feedback further reflect their competitive nature. The interaction of these two processes drives the overall~~ 3F). Collectively, the two branches determine the diurnal variation ~~in~~ of the overall LWP adjustments ~~(black line in Figure 1F).~~.

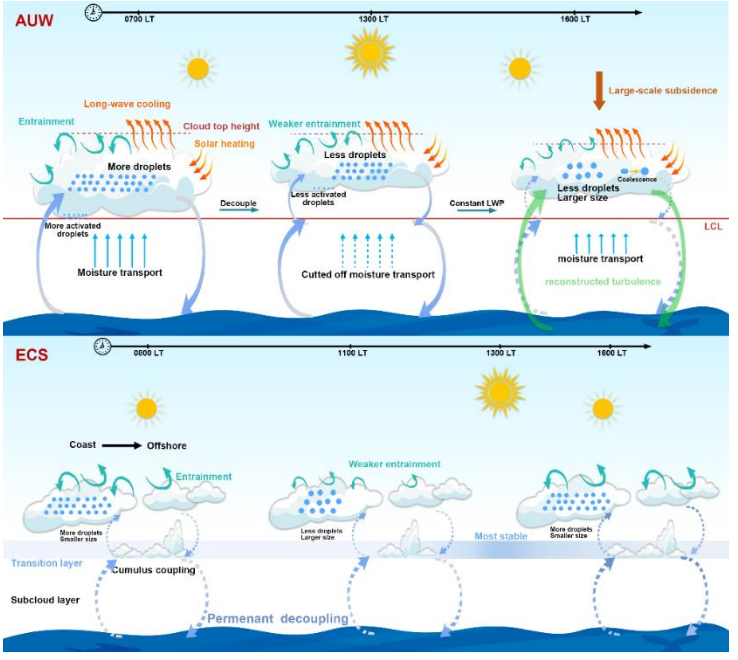

~~**Figure 8. Schematics of diurnal dominant mechanisms observed in AUW and ECS regions. See text for details.** Only the primary mechanisms are presented, while the relatively unimportant ones are omitted. Note that we represent the lifting condensation level (LCL) and transition layer at the same altitude for intuition. However, this depiction does not imply that their heights remain constant throughout the diurnal variation.~~

Given that the samples ~~include four seasons over~~span four years~~, we conduct~~ across all seasons, a sensitivity analysis ~~regarding~~was conducted to assess the impact of seasonal ~~influences as cloud properties and environmental conditions can vary significantly across different seasons.~~variations. Overall, the diurnal LWP adjustment pattern ~~of LWP adjustments~~ is not sensitive to seasonal changes in the AUW region (black lines in ~~Figure~~Figs. ~~S9F-S12F~~S13F-S16F compared to ~~Figure~~Fig. ~~1~~3F). Since the AUW region is a persistent stratocumulus area, the diurnal variations of cloud thickness remain consistent across all seasons, with the thickest clouds in the morning and the thinnest in the early afternoon, followed by a slow increase.

~~This implies~~It suggests that the decoupling process in the persistent Sc region is ~~not affected by seasonality, resulting in~~insensitive to the seasonal changes, leading to similar patterns of LWP adjustments. The ECS region exhibits seasonal differences (Fig~~ure~~s. ~~S9-S12~~S13-S16). Among the total samples (173181), spring, summer, autumn, and winter account for 31%, 3%, 22%, and 44%, respectively. Due to the limited summer samples (3%), their results are ~~statistical insignificance ($p > 0.05$),~~statistically insignificant, especially after eliminating the samples with precipitation by applying the threshold (GPM = 0 mm hr^{-1}). The LWP adjustments in other seasons exhibit similar diurnal patterns and magnitudes, peaking at noon (black lines in Fig~~ure~~s. ~~S9F, S11-S12F~~S13F, S15-S16F). This similarity may be due to the weak seasonal variations in the diurnal patterns of LWP and N_d (not shown). The diurnal patterns of ~~warm invigoration in~~the ascending branch of the V shape during spring and winter ~~are similar to~~align with the overall results (blue lines in Fig~~ure~~s. ~~S9F~~S13F and ~~S12F~~S16F compared to ~~Figure~~Fig. ~~1F~~3F). The N_d minimum ~~N_d~~occurring at 1100 LT coincides with the weakest ~~warm invigoration (i.e., minimal~~positive LWP ~~enhancement). Autumn~~adjustments in the ascending branch. Among all seasons, autumn exhibits the lowest N_d ~~among seasons (Figure S11F),~~, corresponding to the weakest ~~warm invigoration~~positive LWP adjustments in the ascending branch (~50%/31% lower than spring/winter) and the largest diurnal fluctuations~~.~~ (Fig. S15F). This may be attributed to the weakest cold air advection during autumn (Fig. S6). The diurnal pattern of ~~entrainment feedbacks~~the descending branch in spring differs from other seasons~~,~~ (purple line in Fig. S13F), possibly due to ~~its distinct entrainment rate~~ the diurnal variation~~,~~ of entrainment rate which can be illustrated by the variation of ~~cloud-top height (~~CLTH~~)~~. Here, based on the relationship between CLTH, w_s (always negative) and entrainment rate (w_e) ($\frac{dCLTH}{dt} = w_s + w_e$) ~~(Painemal et al., 2013)~~(Painemal et al., 2017), the diurnal variations of w_e (entrainment rate) can be qualitatively analyzed with the diurnal variations of CLTH and large-scale subsidence (w_s) (~~Figure~~Fig. ~~S13~~S17). Before 1400 LT, the variation of large-scale subsidence is unrelated to CLTH, thus the change in CLTH can only be attributed to the entrainment rate. ~~It~~The entrainment rate weakens before 1200 LT, ~~possibly due~~leading to ~~the decreasing cloud-top longwave cooling after sunrise.~~a weakening of the negative LWP adjustments. It then ~~increases~~strengthens until 1400 LT, which ~~may be caused by the enhanced longwave cooling.~~enhances the negative LWP adjustments. After 1400 LT, the observed decrease in CLTH is ~~caused by the enhancement of~~ mainly attributed to an increase in large-scale subsidence. The enhanced subsidence further suppresses the entrainment rate, thereby weakening the negative LWP adjustments.

To summarize, Figure ~~8~~6 depicts schematics of the dominant mechanisms in the two regions. In the AUW region, the primary mechanism behind the diurnal variation of LWP adjustments is the cloud thinning driven by MBL decoupling before 1300 LT. After 1300 LT, the gradual weakening of cloud-top entrainment mitigates the negative LWP adjustments. ~~In ECS region, the~~ The diurnal variation of LWP adjustments in the ECS region is jointly determined by ~~competing~~the ascending and descending branches of the V shape, which is linked to the microphysical~~-dynamical~~ processes ~~(i.~~responsible for the diurnal variations of N_d (e.g., entrainment ~~feedback and warm invigoration~~drying). Failure to accurately capture these diurnal variations in LWP adjustments and the underlying physical processes in observational studies may result in substantial inaccuracies in the quantification of regional and global LWP adjustments, and the associated radiative forcing.

~~3.2 Impacts on aerosol indirect radiative effect if neglecting diurnal variations~~

~~Regional geostationary satellite observation reveals the significant impact of regional diurnal dynamic processes on LWP adjustments. LWP adjustments vary from −0.41 to −0.27 in AUW and from −0.11 to 0.21 in ECS. Diurnal averaged LWP adjustments are −0.31 and 0.02 considering the diurnal processes, respectively. The averaged LWP adjustment (dashed line in Figure 1, C and F) is not a simple average of the values, rather, it is derived from all available data within the region, accounting for diurnal covariation. This implies the inadequacy of previous observations only based on polar-orbiting satellites. For example, for Sc in AUW region, if LWP adjustments observed by polar-orbiting satellite (such as MODIS overpass for aqua at 1330 LT or terra at 1030 LT) are applied to represent the whole day, the negative LWP adjustments will be obviously overestimated because the polar-orbiting observations failed to capture the weaker entrainment process in the late afternoon. This bias will ultimately affect our estimation of cloud brightening in Twomey effect. The cloud albedo (A_c) susceptibility to aerosols can be estimated as (Bellouin et al. 2020)~~

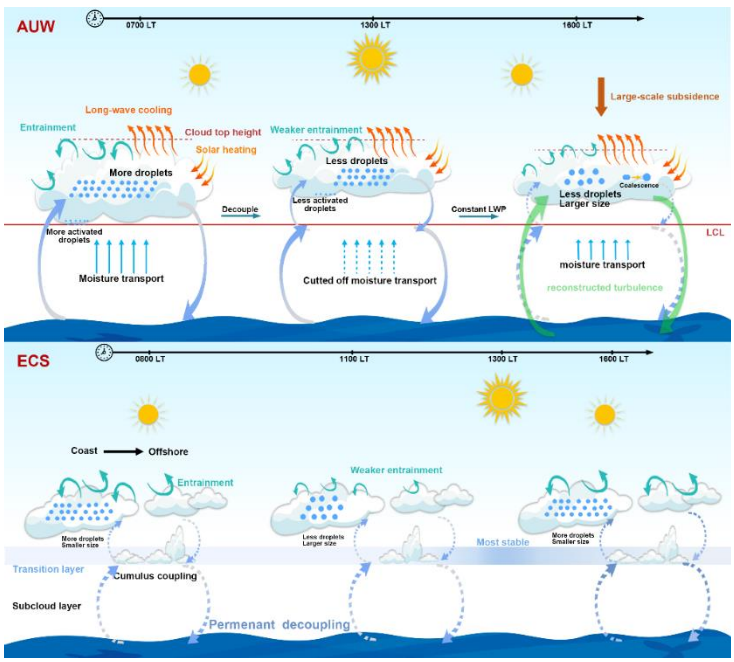

Figure 6: Schematics of diurnal dominant mechanisms observed in the AUW and ECS. See text for details. Only the primary mechanisms are presented, while the relatively unimportant ones are omitted. Note that we represent the lifting condensation level (LCL) and transition layer at the same altitude for intuition. However, this depiction does not imply that their heights remain constant throughout the diurnal variation.

~~:~~

$$S = \frac{dA_c}{dN_d} = \frac{A_c(1 - A_c)}{3N_d}\left(1 + \frac{5}{2}\frac{d\ln LWP}{d\ln N_d}\right) \tag{6}$$

~~where S is the sensitivity of cloud albedo. According to this equation, LWP adjustments serve to regulate the cooling effect of~~

~~the Twomey effect (the first term).~~

~~Following the method of (Glassmeier et al., 2021), we assume that climatological A_c is approximated as a constant value of the steady state. Then the impact of LWP adjustments on S depends on $\left(1+\frac{5}{2}\frac{\mathrm{d}\ln \mathrm{LWP}}{\mathrm{d}\ln \mathrm{N_d}}\right)$ according to Eq. 6. If we only consider LWP adjustments at fixed moments but neglect the diurnal variations, the cooling effect of LWP adjustments (strengthen Twomey effect) will be severely underestimated. For example, the average LWP adjustments at MODIS Aqua and Terra overpasses (1030 LT and 1330 LT) are −0.39 in AUW region and -0.04 in ECS region, respectively. The daily average LWP adjustments for the two regions are −0.31 and 0.02, respectively. After substituting these values into $\left(1+\frac{5}{2}\frac{\mathrm{d}\ln \mathrm{LWP}}{\mathrm{d}\ln \mathrm{N_d}}\right)$, the cooling effect of LWP adjustments will be underestimated by |(0.225−0.025)/0.225|×100% = 89% in AUW region if neglecting the diurnal variations. This bias will lead to a further |(−0.39−(−0.31))/(−0.4)|×100% = 20% offset of the Twomey effect, as the Twomey effect is completely offset when the LWP adjustment is −0.4. Thereby the offset will steer aerosol indirect radiative effect towards a warming direction. Similarly, these two estimates are 14% and 15% for ECS region.~~

~~4 Discussion~~4 Discussion

As discussed above, regional geostationary observations reveal the significant impact of regional diurnal dynamic processes on LWP adjustments, ranging from –0.41 to –0.27 in the AUW and from –0.11 to 0.21 in the ECS. Assuming a constant LWP adjustment based on polar-orbiting snapshots, rather than considering its diurnal variations will ultimately affect the estimation of the aerosol indirect effect. The cloud albedo (A_c) susceptibility to aerosols perturbations is estimated as (Bellouin et al. 2020):

$$S=\frac{\mathrm{d}A_C}{\mathrm{d}\ln \mathrm{N_d}}=\frac{A_C(1-A_C)}{3}\left(1+\frac{5}{2}\frac{\mathrm{d}\ln \mathrm{LWP}}{\mathrm{d}\ln \mathrm{N_d}}\right) \tag{6}$$

where S is the sensitivity of cloud albedo to N_d. A_c is calculated from τ based on a general expression for two-stream approximation solution (Glenn et al., 2020):

$$A_c=\frac{\tau}{13.33+\tau} \tag{7}$$

The first term of Eq. (6) refers to the changes in albedo due to the changes in N_d, while holding the LWP (i.e. Twomey effect). The second term, which accounts for LWP adjustment, can regulate the Twomey effect. The Twomey effect is completely offset when $\frac{\mathrm{d}\ln \mathrm{LWP}}{\mathrm{d}\ln \mathrm{N_d}}$ equals –2/5. Figure 7 shows the diurnal variations of S, calculated with Eq. (6) using the diurnal variations of both A_c and LWP adjustments. To isolate their individual influence, S was calculated using MODIS-averaged value for either A_c or LWP adjustments while retaining the diurnal variation for the other (Fig. S18). Given the minimal diurnal fluctuation in $\frac{A_C(1-A_C)}{3}$, the diurnal variations of S are mainly controlled by LWP adjustments. According to Fig. 7, if S is evaluated only at fixed moments (e.g. the average value during MODIS overpasses for Terra at 1030 LT and Aqua at 1330 LT), the cooling effect of S is consistently underestimated before 1100 LT, with a maximum bias of 89% at 0800 LT. At 1300

LT, S even turns negative, suggesting that albedo decreases with increasing N_d, which has been reported in previous studies (Zhang et al., 2022). The negative S is possibly linked to strong decoupling over the AUW region at 1300 LT as discussed in Section 3.2. In the ECS region, the associated bias spans from a 24% overestimation at 0800 LT to a 40% underestimation at 1600 LT. The results highlight the critical need to account for diurnal variations of LWP adjustments when assessing the aerosol indirect effect. Future studies should incorporate geostationary observations or high-resolution simulations to better constrain the diurnal effects of LWP adjustments.

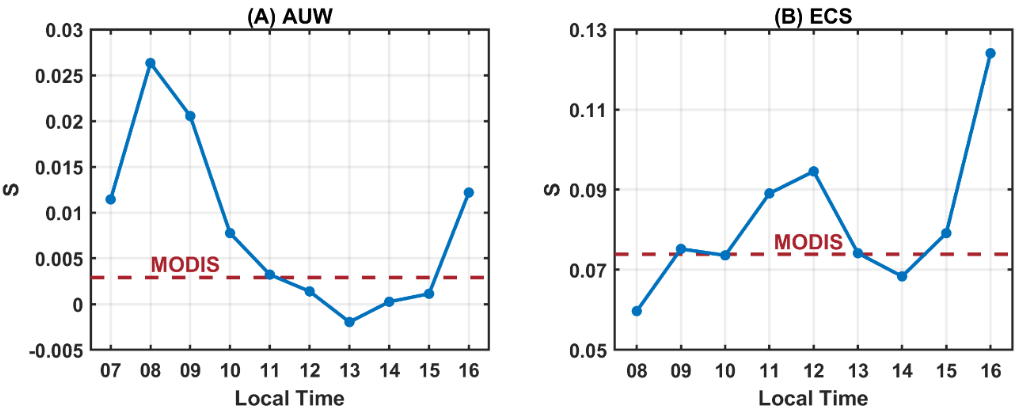

Figure 7: The diurnal variations of S calculated by Eq. (6) in the (A) AUW and (B) ECS (blue lines). The red dashed lines represent the average values during MODIS Terra (1030 LT) and Aqua (1330 LT) overpasses.

Our observed diurnal LWP adjustment pattern in the AUW region is consistent with Qiu et al. (2024)'s findings in the eastern North Atlantic, where thick-thin cloud transitions dominated daytime variability. However, ~~unlike~~the main drivers emphasized in the two studies are different. Qiu et al. (2024)~~'s method, which focused on regional cloud internal evolution and~~ calculated LWP adjustment within each 1° grid box ~~without considering~~ to minimize the meteorological covariations~~, this investigation preserves the influence of meteorological~~ and highlighted cloud-intrinsic evolution, whereas we retain these covariations ~~at each moment. By stratifying analyses~~ and then disentangle their influence by cloud thickness ~~according to~~stratification analyses following Rosenfeld et al. (2019~~),~~). Consequently, we ~~disentangle~~attribute the diurnal variations in LWP adjustments mainly to temporal changes in meteorological ~~covariations from cloud internal feedbacks.~~and dynamical conditions. Additionally, after 1300 LT, cloud thickness remains relatively stable~~ after 1300 LT in our results. The~~ ; the weakening of negative LWP adjustments is ~~primarily due~~linked to ~~the weakening of~~reduced entrainment ~~induced by the strengthening of~~ as large-scale subsidence~~.~~

strengthens (Fig. 4A). Furthermore, we conduct the same analyses in the ECS region with a completely different environmental background~~,~~ and obtain entirely different results. ~~In humid and unstable environments, aerosol-induced warm invigoration is more likely to occur. In this condition, cloud thickness is no longer suitable for distinguishing meteorological conditions as a mediator of~~ The N_d-LWP relationship~~.~~ exhibits a V shape pattern, contrasting with the inverted-V shape reported in previous studies. The ~~cloud thinning mechanism is also insufficient to explain the diurnal variations of LWP adjustments~~discrepancy likely results from the covariations induced by the geographical dependence of samples. This demonstrates that the significant regional differences in the diurnal variations of LWP adjustments, depending on aerosol loadings, cloud regimes and meteorological conditions.

~~It is worth noting that our results also reveal diurnal variations of N_d, a core indicator in ACI, which are also attributed to the MBL diurnal processes. While previous studies have analyzed the long-term variations of N_d, highlighting the key role of aerosols (Hu et al., 2021; Li et al., 2018; McCoy et al., 2015, 2018; Quaas et al., 2006), unexpectedly, there is no good consistency between them in diurnal variations. This discrepancy may stem from previous polar-orbiting satellite observations at fixed times have overlooked the crucial role played by other physical mechanisms at different times. Figure 5 suggests a pronounced impact of anthropogenic activities on cloud microphysical properties on a long-term scale. Note that the correlations between AOD and N_d at certain fixed times are not statistically significant (not shown). This may be due to the relatively insignificant impact of aerosol effects at these moments, while other physical processes may exert a more pronounced influence. Future researches should broaden its scope to investigate effects of other physical processes on N_d at specific times, in addition to the roles of aerosols. Moreover, in the context of global warming, whether these physical processes will be affected and consequently contribute to variations of N_d deserves further investigation.~~

~~Several limitations should be acknowledged in this study. First, the time-dependence of LWP adjustments we discussed differs from the cloud evolution process, emphasizing diurnal variations caused by changes in dominant mechanisms at different times rather than tracking the evolution of individual clouds. This approach may introduce uncertainties into our results since the full cloud life cycle and evolution are not the same with diurnal variations. The full cloud lifetime evolution associated with LWP adjustments is not the scope of this study and warrants further exploration.~~

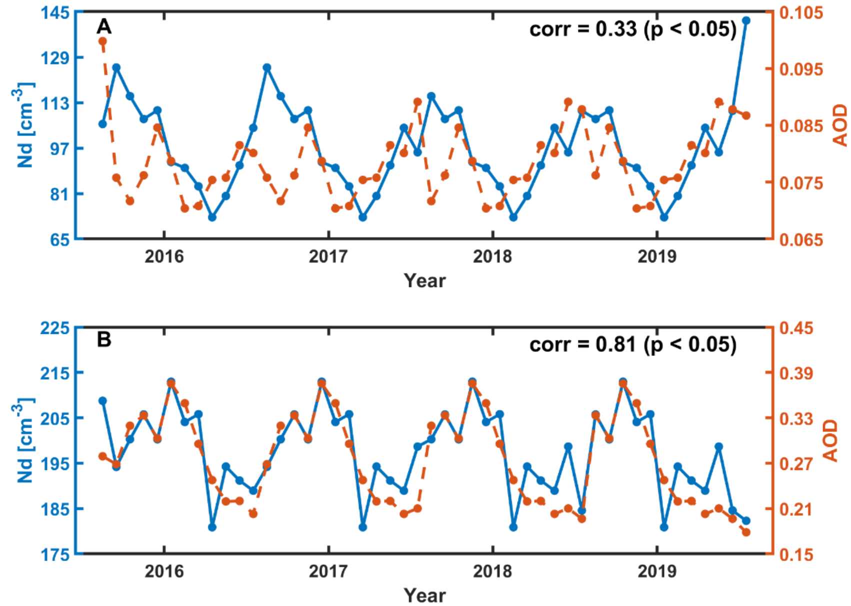

Figure 8: 4-year long-term variations of N_d and aerosol optical depth (AOD) from MERRA-2 at 1200 LT in the AUW (A) and ECS (B) region. The correlation coefficients (corr) between N_d and AOD are 0.33 and 0.81 (significant at the 95% confidence level), respectively.

It is worth noting that our results also reveal diurnal variations of N_d, a core indicator in ACI, which are also attributed to the MBL diurnal processes. While previous studies have analyzed the long-term variations of N_d, highlighting the key role of aerosols (Hu et al., 2021; Li et al., 2018; McCoy et al., 2015, 2018; Quaas et al., 2006), there is no good consistency between them in diurnal variations. This discrepancy may stem from previous polar-orbiting satellite observations at fixed times have overlooked the crucial role played by other physical mechanisms at different times. Figure 8 shows significant correlations observed between the 4-year long-term variations of AOD and N_d at 1200 LT in both regions, particularly in the ECS with a correlation of 0.81. Meanwhile, both regions show the similar distribution patterns, with higher N_d and smaller r_e near the continental coastal area, aligning with the average AOD spatial distribution (spatial correlation coefficients of 0.84 in the AUW and 0.91 in the ECS) (Fig. S1), suggesting a pronounced impact of anthropogenic activities on cloud microphysical properties on a long-term scale. Note that the correlations between AOD and N_d at certain fixed times are not statistically significant (not shown). This may be due to the relatively insignificant impact of aerosol effects at these moments, while other processes may exert a more pronounced influence. For example, strong boundary layer decoupling inhibits cloud droplet activations (Zeider et al., 2025). Mesoscale cloud organization can also introduce spatial heterogeneity in N_d independent of aerosol loading (Zhou and Feingold, 2023). Future research should broaden its scope to investigate the effects of other influencing factors on N_d at specific times, in addition to the role of aerosols. Moreover, in the context of global warming, whether these physical processes will be affected and consequently contribute to variations of N_d deserves further investigation.

Several limitations should be acknowledged in this study. First, the time-dependence of LWP adjustments we discussed differs from the cloud evolution process, emphasizing diurnal variations caused by changes in dominant mechanisms at different times rather than tracking the evolution of individual clouds. This approach may introduce uncertainties into our results since the full cloud life cycle and evolution are not the same with diurnal variations. The full cloud lifetime evolution associated with LWP adjustments is not within the scope of this study and warrants further exploration. Additionally, given the scarcity of observational data at fine scales, certain mechanisms are indirectly inferred from the observational index (e.g., decoupling process inferred from LWP skewness), which needs further microphysical-process-based in-situ observations as well as model simulations. Finally, uncertainties of retrievals have been discussed in Data and Methods, which provides further context for the limitations of this study.

5 Conclusion

This study reveals the diurnal variations of LWP adjustments ~~in two specific regions within the sight of Himawari-8, along with~~and the possible mechanisms contributing to these variations~~. The studied~~ in two specific regions ~~have~~with significant differences in cloud regimes, environmental conditions, and aerosol loadings. ~~Although some conclusions are similar to the previous studies, we have also discovered some new phenomena. The observational studies demonstrate LWP adjustments in two regions are determined by the dominant microphysical-dynamical processes in different N_d stages (entrainment feedbacks and warm invigoration), while their diurnal variations depend on the dynamical conditions of the boundary layer.~~ Important findings from this investigation are as follows:

(1) In the AUW region, the~~ diurnal variations of LWP adjustments are insensitive to seasonality. The~~ overall negative LWP adjustments decrease from −0.27 to −0.41 before 1300 LT and then increase to −0.34. The diurnal variations of LWP adjustments are insensitive to seasonality. Cloud thickness in the AUW region ~~can serve~~serves as a confounder to separate the effects of meteorological covariations. The diurnal pattern is primarily associated with cloud thinning induced by decoupling process of MBL quantified by LWP skewness before 1300 LT and the weakening of entrainment induced by the intensification of large-scale subsidence after 1300 LT.

(2) In the ECS region, ~~diurnal variations of~~LWP increases at high N_d (> ~300 cm^{-3}), leading to a V shape pattern of N_d-LWP relationship. Our results demonstrate a distinct transition in environmental conditions across the turning point of the V shape, indicating the V shape pattern is the result of meteorological covariations. Specifically, the aerosol-rich, relatively cold and dry air from continent reduces the stability of the sub-cloud layer, triggering the release of water vapor into the boundary layer and subsequently promoting cloud droplet activation and development of thicker clouds. These processes collectively lead to an increase in both N_d and LWP, resulting in a positive LWP adjustment at high N_d. The diurnal variations of LWP adjustments exhibit seasonal differences. Samples from winter and spring dominate the overall variations (accounting for 75% of the total samples). ~~For the overall results, LWP increases and~~

~~then decreases with N_d, suggesting possible competition between entrainment feedbacks and warm invigoration. The diurnal pattern of LWP adjustments~~The diurnal LWP adjustment pattern is determined by the combined diurnal variations of ~~these two mechanisms. Warm invigoration is related~~the ascending and descending branches of the V shape, which is likely attributed to the diurnal variation of ~~the N_d at the turning points of the two processes. Lower N_d in the ECS region implies a weaker warm invigoration.~~N_d induced by entrainment.

(3) ~~We~~The results indicate an ~~overall~~ underestimation of the ~~cooling effect by LWP adjustment up to 89% (14%), with a further 20% (15%) offset of the Twomey effect when neglecting the diurnal variations of LWP adjustments in AUW (ECS) region~~cloud albedo sensitivity to aerosol perturbations by up to 89% in the AUW region, while in the ECS region, the bias ranges from a 24% overestimation at 0700 LT to a 40% underestimation at 1600 LT. Furthermore, our results quantify the regional impact of boundary layer dynamic conditions on LWP adjustments. For example, the diurnal decoupling process in the AUW region results in a 219% variation of LWP adjustments within the daytime relative to the daily mean (the diurnal variation range divided by the daily mean), assuming other conditions remain relatively unchanged.

Our research provides a detailed discussion for the diurnal variations of LWP adjustments and how they are influenced by existed boundary layer mechanisms. We underscore the importance of fully considering the ~~covariation~~covariations with environmental conditions, indicating different potential influencing factors on cloud brightening and radiative forcing in terms of the regional and diurnal daytime scale. It is a highly time-dependent variable lacking quantification and should be taken into consideration of future research in aerosol indirect effects on climate.

Data availability

The datasets that support this study are all available to the public. The SatCORPS Himawari-8 product is available at https://asdc.larc.nasa.gov/project/CERES. The MERRA-2 product is available at https://disc.gsfc.nasa.gov/datasets/M2T1NXAER_5.12.4/summary?keywords=merra2. The GPM_3IMERGHHV07 is available at https://disc.gsfc.nasa.gov/datasets/GPM_3IMERGHH_07/summary?keywords=gpm%20imerg. ERA5 reanalysis data ~~is~~are available at https://cds.climate.copernicus.eu/. All data are available in the main text or the supporting information.

Author contributions

JiaL and YaW performed the analysis and organized the original manuscript. JimL and YaW conceptualized the study and reviewed the manuscript. WZ assisted in data analysis and validation. LZ and YuW assisted in the investigation and the final review and editing of the manuscript.

Competing interests

The contact author has declared that none of the authors has any competing interests.

Acknowledgments

We would like to acknowledge ChatGPT for its role in polishing the language for the text. We would like to acknowledge freepik.com for supporting icons used in our schematics (www.freepik.com).

Financial support

This work is supported by the following funding: Key Program of the National Natural Science Foundation of China (42430601), Major Program of the National Natural Science Foundation of China (42090030), National Natural Science Foundation of China (42175087), Science and Technology Project of Gansu Province (Outstanding Youth Fund, 24JRRA386).

References

Ackerman, A. S., Kirkpatrick, M. P., Stevens, D. E., and Toon, O. B.: The impact of humidity above stratiform clouds on indirect aerosol climate forcing, Nature, 432, 1014–1017, https://doi.org/10.1038/nature03174, 2004.

Albrecht, B. A.: Aerosols, Cloud Microphysics, and Fractional Cloudiness, Science, 245, 1227–1230, https://doi.org/10.1126/science.245.4923.1227, 1989.

Albrecht, B. A., Bretherton, C. S., Johnson, D., Scubert, W. H., and Frisch, A. S.: The Atlantic Stratocumulus Transition Experiment—ASTEX, Bulletin of the American Meteorological Society, 76, 889–904, https://doi.org/10.1175/1520-0477(1995)076<0889:TASTE>2.0.CO;2, 1995.

~~Altaratz, O., Koren, I., Remer, L. A., and Hirsch, E.: Review: Cloud invigoration by aerosols—Coupling between microphysics and dynamics, Atmospheric Research, 140–141, 38–60, https://doi.org/10.1016/j.atmosres.2014.01.009, 2014.~~

Bellouin, N., Quaas, J., Gryspeerdt, E., Kinne, S., Stier, P., Watson-Parris, D., Boucher, O., Carslaw, K. S., Christensen, M., Daniau, A. -L., Dufresne, J. -L., Feingold, G., Fiedler, S., Forster, P., Gettelman, A., Haywood, J. M., Lohmann, U., Malavelle, F., Mauritsen, T., McCoy, D. T., Myhre, G., Mülmenstädt, J., Neubauer, D., Possner, A., Rugenstein, M., Sato, Y., Schulz, M., Schwartz, S. E., Sourdeval, O., Storelvmo, T., Toll, V., Winker, D., and Stevens, B.: Bounding Global Aerosol Radiative Forcing of Climate Change, Rev. Geophys., 58, https://doi.org/10.1029/2019RG000660, 2020.

Bender, F. A.-M., Frey, L., McCoy, D. T., Grosvenor, D. P., and Mohrmann, J. K.: Assessment of aerosol–cloud–radiation correlations in satellite observations, climate models and reanalysis, Clim Dyn, 52, 4371–4392, https://doi.org/10.1007/s00382-018-4384-z, 2019.

Bennartz, R.: Global assessment of marine boundary layer cloud droplet number concentration from satellite, J. Geophys. Res., 112, D02201, https://doi.org/10.1029/2006JD007547, 2007.

Bennartz, R. and Rausch, J.: Global and regional estimates of warm cloud droplet number concentration based on 13 years of AQUA-MODIS observations, Atmos. Chem. Phys., 17, 9815–9836, https://doi.org/10.5194/acp-17-9815-2017, 2017.

Boers, R., Acarreta, J. R., and Gras, J. L.: Satellite monitoring of the first indirect aerosol effect: Retrieval of the droplet concentration of water clouds, Journal of Geophysical Research: Atmospheres, 111, https://doi.org/10.1029/2005JD006838, 2006.

Bougeault, P.: The Diurnal Cycle of the Marine Stratocumulus Layer: A Higher-Order Model Study, Journal of the Atmospheric Sciences, 42, 2826–2843, https://doi.org/10.1175/1520-0469(1985)042<2826:TDCOTM>2.0.CO;2, 1985.

Brenguier, J.-L., Burnet, F., and Geoffroy, O.: Cloud optical thickness and liquid water path – does the *k* coefficient vary with droplet concentration?, Atmospheric Chemistry and Physics, 11, 9771–9786, https://doi.org/10.5194/acp-11-9771-2011, 2011.

Bretherton, C. S~~. and Wyant, M. C.: Moisture Transport, Lower-Tropospheric Stability, and Decoupling of Cloud-Topped Boundary Layers, Journal of the Atmospheric Sciences, 54, 148–167, https://doi.org/10.1175/1520-0469(1997)054<0148:MTLTSA>2.0.CO;2, 1997.~~

~~Bretherton, C. S~~., Uttal, T., Fairall, C. W., Yuter, S. E., Weller, R. A., Baumgardner, D., Comstock, K., Wood, R., and Raga, G. B.: The Epic 2001 Stratocumulus Study, Bulletin of the American Meteorological Society, 85, 967–978, https://doi.org/10.1175/BAMS-85-7-967, 2004.

Bretherton, C. S., Blossey, P. N., and Uchida, J.: Cloud droplet sedimentation, entrainment efficiency, and subtropical stratocumulus albedo, Geophysical Research Letters, 34, 2006GL027648, https://doi.org/10.1029/2006GL027648, 2007.

Buchard, V., Randles, C. A., Silva, A. M. da, Darmenov, A., Colarco, P. R., Govindaraju, R., Ferrare, R., Hair, J., Beyersdorf, A. J., Ziemba, L. D., and Yu, H.: The MERRA-2 Aerosol Reanalysis, 1980 Onward. Part II: Evaluation and Case Studies, Journal of Climate, 30, 6851–6872, https://doi.org/10.1175/JCLI-D-16-0613.1, 2017.

Caldwell, P., Bretherton, C. S., and Wood, R.: Mixed-Layer Budget Analysis of the Diurnal Cycle of Entrainment in Southeast Pacific Stratocumulus, Journal of the Atmospheric Sciences, 62, 3775–3791, https://doi.org/10.1175/JAS3561.1, 2005.

Change (IPCC), I. P. on C.: The Earth's Energy Budget, Climate Feedbacks and Climate Sensitivity, in: Climate Change 2021 – The Physical Science Basis: Working Group I Contribution to the Sixth Assessment Report of the Intergovernmental Panel on Climate Change, Cambridge University Press, 923–1054, 2023.

Chen, Y., Haywood, J., Wang, Y., Malavelle, F., Jordan, G., Partridge, D., Fieldsend, J., De Leeuw, J., Schmidt, A., Cho, N., Oreopoulos, L., Platnick, S., Grosvenor, D., Field, P., and Lohmann, U.: Machine learning reveals climate forcing from aerosols is dominated by increased cloud cover, Nat. Geosci., 15, 609–614, https://doi.org/10.1038/s41561-022-00991-6, 2022.

Chen, Y.-C., Christensen, M. W., Stephens, G. L., and Seinfeld, J. H.: Satellite-based estimate of global aerosol–cloud radiative forcing by marine warm clouds, Nature Geosci, 7, 643–646, https://doi.org/10.1038/ngeo2214, 2014.

Christensen, M. W. and Stephens, G. L.: Microphysical and macrophysical responses of marine stratocumulus polluted by underlying ships: Evidence of cloud deepening, J. Geophys. Res., 116, D03201, https://doi.org/10.1029/2010JD014638, 2011.

Coakley, J. A. and Walsh, C. D.: Limits to the Aerosol Indirect Radiative Effect Derived from Observations of Ship Tracks, Journal of the Atmospheric Sciences, 59, 668–680, https://doi.org/10.1175/1520-0469(2002)059<0668:LTTAIR>2.0.CO;2, 2002.

~~Dagan, G., Koren, I., and Altaratz, O.: Competition between core and periphery-based processes in warm convective clouds – from invigoration to suppression, Atmospheric Chemistry and Physics, 15, 2749–2760, https://doi.org/10.5194/acp-15-2749-2015, 2015.~~

Duynkerke, P. G. and Hignett, P.: Simulation of Diurnal Variation in a Stratocumulus-capped Marine Boundary Layer during FIRE, Monthly Weather Review, 121, 3291–3300, https://doi.org/10.1175/1520-0493(1993)121<3291:SODVIA>2.0.CO;2, 1993.

~~Engström, A. and Ekman, A. M. L.: Impact of meteorological factors on the correlation between aerosol optical depth and cloud fraction: IMPACTS ON AEROSOL-CLOUD RELATIONSHIPS, Geophys. Res. Lett., 37, n/a-n/a, https://doi.org/10.1029/2010GL044361, 2010.~~

Feingold, G., Ghate, V. P., Russell, L. M., Blossey, P., Cantrell, W., Christensen, M. W., Diamond, M. S., Gettelman, A., Glassmeier, F., Gryspeerdt, E., Haywood, J., Hoffmann, F., Kaul, C. M., Lebsock, M., McComiskey, A. C., McCoy, D. T., Ming, Y., Mülmenstädt, J., Possner, A., Prabhakaran, P., Quinn, P. K., Schmidt, K. S., Shaw, R. A., Singer, C. E., Sorooshian, A., Toll, V., Wan, J. S., Wood, R., Yang, F., Zhang, J., and Zheng, X.: Physical science research needed to evaluate the viability and risks of marine cloud brightening, Sci. Adv., 10, eadi8594, https://doi.org/10.1126/sciadv.adi8594, 2024.

Feingold, G., Glassmeier, F., Zhang, J., and Hoffmann, F.: Opinion: Inferring Process from Snapshots of Cloud Systems, EGUsphere, 1–28, https://doi.org/10.5194/egusphere-2025-1869, 2025.

Fons, E., Runge, J., Neubauer, D., and Lohmann, U.: Stratocumulus adjustments to aerosol perturbations disentangled with a causal approach, npj Clim Atmos Sci, 6, 130, https://doi.org/10.1038/s41612-023-00452-w, 2023.

George, R. C. and Wood, R.: Subseasonal variability of low cloud radiative properties over the southeast Pacific Ocean, Atmos. Chem. Phys., 10, 4047–4063, https://doi.org/10.5194/acp-10-4047-2010, 2010.

Ghosh, S., Osborne, S., and Smith, M. H.: On the importance of cumulus penetration on the microphysical and optical properties of stratocumulus clouds, Atmospheric Chemistry and Physics, 5, 755–765, https://doi.org/10.5194/acp-5-755-2005, 2005.

Glassmeier, F., Hoffmann, F., Johnson, J. S., Yamaguchi, T., Carslaw, K. S., and Feingold, G.: Aerosol-cloud-climate cooling overestimated by ship-track data, Science, 371, 485–489, https://doi.org/10.1126/science.abd3980, 2021.

Glenn, I. B., Feingold, G., Gristey, J. J., and Yamaguchi, T.: Quantification of the Radiative Effect of Aerosol–Cloud Interactions in Shallow Continental Cumulus Clouds, https://doi.org/10.1175/JAS-D-19-0269.1, 2020.

Goren, T., Choudhury, G., Kretzschmar, J., and McCoy, I.: Co-variability drives the inverted-V sensitivity between liquid water path and droplet concentrations, Atmospheric Chemistry and Physics, 25, 3413–3423, https://doi.org/10.5194/acp-25-3413-2025, 2025.

Grosvenor, D. P., Sourdeval, O., Zuidema, P., Ackerman, A., Alexandrov, M. D., Bennartz, R., Boers, R., Cairns, B., Chiu, J. C., Christensen, M., Deneke, H., Diamond, M., Feingold, G., Fridlind, A., Hünerbein, A., Knist, C., Kollias, P., Marshak, A., McCoy, D., Merk, D., Painemal, D., Rausch, J., Rosenfeld, D., Russchenberg, H., Seifert, P., Sinclair, K., Stier, P., van Diedenhoven, B., Wendisch, M., Werner, F., Wood, R., Zhang, Z., and Quaas, J.: Remote Sensing of Droplet Number Concentration in Warm Clouds: A Review of the Current State of Knowledge and Perspectives, Reviews of Geophysics, 56, 409–453, https://doi.org/10.1029/2017RG000593, 2018.

Gryspeerdt, E., Goren, T., Sourdeval, O., Quaas, J., Mülmenstädt, J., Dipu, S., Unglaub, C., Gettelman, A., and Christensen, M.: Constraining the aerosol influence on cloud liquid water path, Atmos. Chem. Phys., 19, 5331–5347, https://doi.org/10.5194/acp-19-5331-2019, 2019.

Gryspeerdt, E., Goren, T., and Smith, T. W. P.: Observing the timescales of aerosol–cloud interactions in snapshot satellite images, Atmos. Chem. Phys., 21, 6093–6109, https://doi.org/10.5194/acp-21-6093-2021, 2021.

Gryspeerdt, E., Glassmeier, F., Feingold, G., Hoffmann, F., and Murray-Watson, R. J.: Observing short-timescale cloud development to constrain aerosol–cloud interactions, Atmos. Chem. Phys., 22, 11727–11738, https://doi.org/10.5194/acp-22-11727-2022, 2022a.

Gryspeerdt, E., McCoy, D. T., Crosbie, E., Moore, R. H., Nott, G. J., Painemal, D., Small-Griswold, J., Sorooshian, A., and Ziemba, L.: The impact of sampling strategy on the cloud droplet number concentration estimated from satellite data, Atmos. Meas. Tech., 15, 3875–3892, https://doi.org/10.5194/amt-15-3875-2022, 2022b.

Gryspeerdt, E., Povey, A. C., Grainger, R. G., Hasekamp, O., Hsu, N. C., Mulcahy, J. P., Sayer, A. M., and Sorooshian, A.: Uncertainty in aerosol–cloud radiative forcing is driven by clean conditions, Atmos. Chem. Phys., 23, 4115–4122, https://doi.org/10.5194/acp-23-4115-2023, 2023.

Hersbach, H., Bell, B., Berrisford, P., Hirahara, S., Horányi, A., Muñoz-Sabater, J., Nicolas, J., Peubey, C., Radu, R., Schepers, D., Simmons, A., Soci, C., Abdalla, S., Abellan, X., Balsamo, G., Bechtold, P., Biavati, G., Bidlot, J., Bonavita, M., De Chiara, G., Dahlgren, P., Dee, D., Diamantakis, M., Dragani, R., Flemming, J., Forbes, R., Fuentes, M., Geer, A., Haimberger, L., Healy, S., Hogan, R. J., Hólm, E., Janisková, M., Keeley, S., Laloyaux, P., Lopez, P., Lupu, C., Radnoti, G., de Rosnay, P., Rozum, I., Vamborg, F., Villaume, S., and Thépaut, J.-N.: The ERA5 global reanalysis, Quarterly Journal of the Royal Meteorological Society, 146, 1999–2049, https://doi.org/10.1002/qj.3803, 2020.

Heus, T., Dijk, G. van, Jonker, H. J. J., and Akker, H. E. A. V. den: Mixing in Shallow Cumulus Clouds Studied by Lagrangian Particle Tracking, https://doi.org/10.1175/2008JAS2572.1, 2008.

Hu, Y., Lu, X., Zhai, P.-W., Hostetler, C. A., Hair, J. W., Cairns, B., Sun, W., Stamnes, S., Omar, A., Baize, R., Videen, G., Mace, J., McCoy, D. T., McCoy, I. L., and Wood, R.: Liquid Phase Cloud Microphysical Property Estimates From CALIPSO Measurements, Front. Remote Sens., 2, https://doi.org/10.3389/frsen.2021.724615, 2021.

Huffman, G. J., Bolvin, D. T., Braithwaite, D., Hsu, K.-L., Joyce, R. J., Kidd, C., Nelkin, E. J., Sorooshian, S., Stocker, E. F., Tan, J., Wolff, D. B., and Xie, P.: Integrated Multi-satellite Retrievals for the Global Precipitation Measurement (GPM) Mission (IMERG), in: Satellite Precipitation Measurement: Volume 1, edited by: Levizzani, V., Kidd, C., Kirschbaum, D. B., Kummerow, C. D., Nakamura, K., and Turk, F. J., Springer International Publishing, Cham, 343–353, https://doi.org/10.1007/978-3-030-24568-9_19, 2020.

Jian, B., Li, J., Wang, G., Zhao, Y., Li, Y., Wang, J., Zhang, M., and Huang, J.: Evaluation of the CMIP6 marine subtropical stratocumulus cloud albedo and its controlling factors, Atmos. Chem. Phys., 21, 9809–9828, https://doi.org/10.5194/acp-21-9809-2021, 2021.

Jiang, X., Su, H., Jiang, J. H., Neelin, J. D., Wu, L., Tsushima, Y., and Elsaesser, G.: Muted extratropical low cloud seasonal cycle is closely linked to underestimated climate sensitivity in models, Nat Commun, 14, 5586, https://doi.org/10.1038/s41467-023-41360-0, 2023.

Kang, L., Marchand, R., and Smith, W.: Evaluation of MODIS and Himawari-8 Low Clouds Retrievals Over the Southern Ocean With In Situ Measurements From the SOCRATES Campaign, Earth and Space Science, 8, https://doi.org/10.1029/2020EA001397, 2021.

~~Kaufman, Y. J., Koren, I., Remer, L. A., Rosenfeld, D., and Rudich, Y.: The effect of smoke, dust, and pollution aerosol on shallow cloud development over the Atlantic Ocean, Proc. Natl. Acad. Sci. U.S.A., 102, 11207–11212, https://doi.org/10.1073/pnas.0505191102, 2005.~~

Kazil, J., Yamaguchi, T., and Feingold, G.: Mesoscale organization, entrainment, and the properties of a closed-cell stratocumulus cloud, Journal of Advances in Modeling Earth Systems, 9, 2214–2229, https://doi.org/10.1002/2017MS001072, 2017.

Klein, S. A. and Hartmann, D. L.: The Seasonal Cycle of Low Stratiform Clouds, Journal of Climate, 6, 1587–1606, https://doi.org/10.1175/1520-0442(1993)006<1587:TSCOLS>2.0.CO;2, 1993.

~~Koren, I., Dagan, G., and Altaratz, O.: From aerosol-limited to invigoration of warm convective clouds, Science, 344, 1143–1146, https://doi.org/10.1126/science.1252595, 2014.~~

Li, J., Jian, B., Huang, J., Hu, Y., Zhao, C., Kawamoto, K., Liao, S., and Wu, M.: Long-term variation of cloud droplet number concentrations from space-based Lidar, Remote Sensing of Environment, 213, 144–161, https://doi.org/10.1016/j.rse.2018.05.011, 2018.

~~Manshausen, P., Watson-Parris, D., Christensen, M. W., Jalkanen, J.-P., and Stier, P.: Invisible ship tracks show large cloud sensitivity to aerosol, Nature, 610, 101–106, https://doi.org/10.1038/s41586-022-05122-0, 2022.~~

Liu, J.-W., Xie, S.-P., Yang, S., and Zhang, S.-P.: Low-Cloud Transitions across the Kuroshio Front in the East China Sea, Journal of Climate, 29, 4429–4443, https://doi.org/10.1175/JCLI-D-15-0589.1, 2016.

Long, J., Wang, Y., Zhang, S., and Liu, J.: Transition of Low Clouds in the East China Sea and Kuroshio Region in Winter: A Regional Atmospheric Model Study, Journal of Geophysical Research: Atmospheres, 125, e2020JD032509, https://doi.org/10.1029/2020JD032509, 2020.

Martin, G. M., Johnson, D. W., and Spice, A.: The Measurement and Parameterization of Effective Radius of Droplets in Warm Stratocumulus Clouds, Journal of the Atmospheric Sciences, 51, 1823–1842, https://doi.org/10.1175/1520-0469(1994)051<1823:TMAPOE>2.0.CO;2, 1994.

Martin, G. M., Johnson, D. W., Rogers, D. P., Jonas, P. R., Minnis, P., and Hegg, D. A.: Observations of the Interaction between Cumulus Clouds and Warm Stratocumulus Clouds in the Marine Boundary Layer during ASTEX, Journal of the Atmospheric Sciences, 52, 2902–2922, https://doi.org/10.1175/1520-0469(1995)052<2902:OOTIBC>2.0.CO;2, 1995.

McCoy, D. T., Burrows, S. M., Wood, R., Grosvenor, D. P., Elliott, S. M., Ma, P.-L., Rasch, P. J., and Hartmann, D. L.: Natural aerosols explain seasonal and spatial patterns of Southern Ocean cloud albedo, Sci. Adv., 1, e1500157, https://doi.org/10.1126/sciadv.1500157, 2015.

McCoy, D. T., Bender, F. A.-M., Grosvenor, D. P., Mohrmann, J. K., Hartmann, D. L., Wood, R., and Field, P. R.: Predicting decadal trends in cloud droplet number concentration using reanalysis and satellite data, Atmos. Chem. Phys., 18, 2035–2047, https://doi.org/10.5194/acp-18-2035-2018, 2018.

Mechoso, C. R., Wood, R., Weller, R., Bretherton, C. S., Clarke, A. D., Coe, H., Fairall, C., Farrar, J. T., Feingold, G., Garreaud, R., Grados, C., McWilliams, J., Szoeke, S. P. de, Yuter, S. E., and Zuidema, P.: Ocean–Cloud–Atmosphere–Land Interactions in the Southeastern Pacific: The VOCALS Program, Bulletin of the American Meteorological Society, 95, 357–375, https://doi.org/10.1175/BAMS-D-11-00246.1, 2014.

Mellado, J. P.: Cloud-Top Entrainment in Stratocumulus Clouds, Annu. Rev. Fluid Mech., 49, 145–169, https://doi.org/10.1146/annurev-fluid-010816-060231, 2017.

Michibata, T., Suzuki, K., Sato, Y., and Takemura, T.: The source of discrepancies in aerosol–cloud–precipitation interactions between GCM and A-Train retrievals, Atmos. Chem. Phys., 16, 15413–15424, https://doi.org/10.5194/acp-16-15413-2016, 2016.

Miller, M. A., Jensen, M. P., and Clothiaux, E. E.: Diurnal Cloud and Thermodynamic Variations in the Stratocumulus Transition Regime: A Case Study Using In Situ and Remote Sensors, Journal of the Atmospheric Sciences, 55, 2294–2310, https://doi.org/10.1175/1520-0469(1998)055<2294:DCATVI>2.0.CO;2, 1998.

~~Miller, S. D., Rogers, M. A., Haynes, J. M., Sengupta, M., and Heidinger, A. K.: Short-term solar irradiance forecasting via satellite/model coupling, Solar Energy, 168, 102–117, https://doi.org/10.1016/j.solener.2017.11.049, 2018.~~

Min, Q., Joseph, E., Lin, Y., Min, L., Yin, B., Daum, P. H., Kleinman, L. I., Wang, J., and Lee, Y.-N.: Comparison of MODIS cloud microphysical properties with in-situ measurements over the Southeast Pacific, Atmospheric Chemistry and Physics, 12, 11261–11273, https://doi.org/10.5194/acp-12-11261-2012, 2012.

Minnis, P., Sun-Mack, S., Young, D. F., Heck, P. W., Garber, D. P., Chen, Y., Spangenberg, D. A., Arduini, R. F., Trepte, Q. Z., Smith, W. L., Ayers, J. K., Gibson, S. C., Miller, W. F., Hong, G., Chakrapani, V., Takano, Y., Liou, K.-N., Xie, Y., and Yang, P.: CERES Edition-2 Cloud Property Retrievals Using TRMM VIRS and Terra and Aqua MODIS Data—Part I: Algorithms, IEEE Trans. Geosci. Remote Sensing, 49, 4374–4400, https://doi.org/10.1109/TGRS.2011.2144601, 2011.

Minnis, P., Sun-Mack, S., Chen, Y., Chang, F.-L., Yost, C. R., Smith, W. L., Heck, P. W., Arduini, R. F., Bedka, S. T., Yi, Y., Hong, G., Jin, Z., Painemal, D., Palikonda, R., Scarino, B. R., Spangenberg, D. A., Smith, R. A., Trepte, Q. Z., Yang, P., and Xie, Y.: CERES MODIS Cloud Product Retrievals for Edition 4—Part I: Algorithm Changes, IEEE Transactions on Geoscience and Remote Sensing, 59, 2744–2780, https://doi.org/10.1109/TGRS.2020.3008866, 2021.

NASA/LARC/SD/ASDC: SatCORPS CERES GEO Edition 4 Himawari-8 Northern Hemisphere Version 1.2, 2018a.

NASA/LARC/SD/ASDC: SatCORPS CERES GEO Edition 4 Himawari-8 Southern Hemisphere Version 1.2, 2018b.

Painemal, D. and Zuidema, P.: Assessment of MODIS cloud effective radius and optical thickness retrievals over the Southeast Pacific with VOCALS-REx in situ measurements, Journal of Geophysical Research: Atmospheres, 116, https://doi.org/10.1029/2011JD016155, 2011.

Painemal, D., Minnis, P., and O'Neill, L.: The Diurnal Cycle of Cloud-Top Height and Cloud Cover over the Southeastern Pacific as Observed by GOES-10, Journal of the Atmospheric Sciences, 70, 2393–2408, https://doi.org/10.1175/JAS-D-12-0325.1, 2013.

Painemal, D., Xu, K., Palikonda, R., and Minnis, P.: Entrainment rate diurnal cycle in marine stratiform clouds estimated from geostationary satellite retrievals and a meteorological forecast model, Geophysical Research Letters, 44, 7482–7489, https://doi.org/10.1002/2017GL074481, 2017.

Papritz, L., Pfahl, S., Sodemann, H., and Wernli, H.: A Climatology of Cold Air Outbreaks and Their Impact on Air–Sea Heat Fluxes in the High-Latitude South Pacific, https://doi.org/10.1175/JCLI-D-14-00482.1, 2015.

Qiu, S., Zheng, X., Painemal, D., Terai, C., and Zhou, X.: Diurnal variation of aerosol indirect effect for warm marine boundary layer clouds in the eastern north Atlantic, Clouds and Precipitation/Remote Sensing/Troposphere/Physics (physical properties and processes), https://doi.org/10.5194/egusphere-2023-1676, 2023.

Qiu, S., Zheng, X., Painemal, D., Terai, C. R., and Zhou, X.: Daytime variation in the aerosol indirect effect for warm marine boundary layer clouds in the eastern North Atlantic, Atmospheric Chemistry and Physics, 24, 2913–2935, https://doi.org/10.5194/acp-24-2913-2024, 2024.

Qu, X., Hall, A., Klein, S. A., and DeAngelis, A. M.: Positive tropical marine low-cloud cover feedback inferred from cloud-controlling factors, Geophys. Res. Lett., 42, 7767–7775, https://doi.org/10.1002/2015GL065627, 2015.

Quaas, J., Boucher, O., and Lohmann, U.: Constraining the total aerosol indirect effect in the LMDZ and ECHAM4 GCMs using MODIS satellite data, Atmospheric Chemistry and Physics, 6, 947–955, https://doi.org/10.5194/acp-6-947-2006, 2006.

Rahu, J., Trofimov, H., Post, P., and Toll, V.: Diurnal Evolution of Cloud Water Responses to Aerosols, JGR Atmospheres, 127, https://doi.org/10.1029/2021JD035091, 2022.

Rogers, D. P., Yang, X., Norris, P. M., Johnson, D. W., Martin, G. M., Friehe, C. A., and Berger, B. W.: Diurnal Evolution of the Cloud-Topped Marine Boundary Layer. Part I: Nocturnal Stratocumulus Development, Journal of the Atmospheric Sciences, 52, 2953–2966, https://doi.org/10.1175/1520-0469(1995)052<2953:DEOTCT>2.0.CO;2, 1995.

Rosenfeld, D., Wang, H., and Rasch, P. J.: The roles of cloud drop effective radius and LWP in determining rain properties in marine stratocumulus, Geophysical Research Letters, 39, https://doi.org/10.1029/2012GL052028, 2012.

Rosenfeld, D., Zhu, Y., Wang, M., Zheng, Y., Goren, T., and Yu, S.: Aerosol-driven droplet concentrations dominate coverage and water of oceanic low-level clouds, Science, 363, eaav0566, https://doi.org/10.1126/science.aav0566, 2019.

Rosenfeld, D., Kokhanovsky, A., Goren, T., Gryspeerdt, E., Hasekamp, O., Jia, H., Lopatin, A., Quaas, J., Pan, Z., and Sourdeval, O.: Frontiers in Satellite-Based Estimates of Cloud-Mediated Aerosol Forcing, Reviews of Geophysics, 61, e2022RG000799, https://doi.org/10.1029/2022RG000799, 2023.

Scott, R. C., Myers, T. A., Norris, J. R., Zelinka, M. D., Klein, S. A., Sun, M., and Doelling, D. R.: Observed Sensitivity of Low-Cloud Radiative Effects to Meteorological Perturbations over the Global Oceans, Journal of Climate, 33, 7717–7734, https://doi.org/10.1175/JCLI-D-19-1028.1, 2020.

Slingo, A., Nicholls, S., and Schmetz, J.: Aircraft observations of marine stratocumulus during JASIN, Quart J Royal Meteoro Soc, 108, 833–856, https://doi.org/10.1002/qj.49710845807, 1982.

Small, J. D., Chuang, P. Y., Feingold, G., and Jiang, H.: Can aerosol decrease cloud lifetime?, Geophys. Res. Lett., 36, L16806, https://doi.org/10.1029/2009GL038888, 2009.

Small, J. D., Chuang, P. Y., and Jonsson, H. H.: Microphysical imprint of entrainment in warm cumulus, Tellus B: Chemical and Physical Meteorology, 65, https://doi.org/10.3402/tellusb.v65i0.19922, 2013.

Smalley, K. M., Lebsock, M. D., and Eastman, R.: Diurnal Patterns in the Observed Cloud Liquid Water Path Response to Droplet Number Perturbations, Geophysical Research Letters, 51, e2023GL107323, https://doi.org/10.1029/2023GL107323, 2024.

Sun-Mack, S., Minnis, P., Chen, Y., Kato, S., Yi, Y., Gibson, S. C., Heck, P. W., and Winker, D. M.: Regional Apparent Boundary Layer Lapse Rates Determined from CALIPSO and MODIS Data for Cloud-Height Determination, https://doi.org/10.1175/JAMC-D-13-081.1, 2014.

Toll, V., Christensen, M., Quaas, J., and Bellouin, N.: Weak average liquid-cloud-water response to anthropogenic aerosols, Nature, 572, 51–55, https://doi.org/10.1038/s41586-019-1423-9, 2019.

Towers, S.: Potential fitting biases resulting from grouping data into variable width bins, Physics Letters B, 735, 146–148, https://doi.org/10.1016/j.physletb.2014.06.023, 2014.

Trepte, Q. Z., Minnis, P., Sun-Mack, S., Yost, C. R., Chen, Y., Jin, Z., Hong, G., Chang, F.-L., Smith, W. L., Bedka, K. M., and Chee, T. L.: Global Cloud Detection for CERES Edition 4 Using Terra and Aqua MODIS Data, IEEE Transactions on Geoscience and Remote Sensing, 57, 9410–9449, https://doi.org/10.1109/TGRS.2019.2926620, 2019.

Trofimov, H., Bellouin, N., and Toll, V.: Large-Scale Industrial Cloud Perturbations Confirm Bidirectional Cloud Water Responses to Anthropogenic Aerosols, JGR Atmospheres, 125, https://doi.org/10.1029/2020JD032575, 2020.

Twomey, S.: The Influence of Pollution on the Shortwave Albedo of Clouds, Journal of the Atmospheric Sciences, 34, 1149–1152, https://doi.org/10.1175/1520-0469(1977)034<1149:TIOPOT>2.0.CO;2, 1977.

Marine Low Clouds : Radiation, Turbulence, and Forecasting:

Wang, Y., Zhao, C., McFarquhar, G. M., Wu, W., Reeves, M., and Li, J.: Dispersion of Droplet Size Distributions in Supercooled Non-precipitating Stratocumulus from Aircraft Observations Obtained during the Southern Ocean Cloud Radiation Aerosol Transport Experimental Study, Journal of Geophysical Research: Atmospheres, 126, e2020JD033720, https://doi.org/10.1029/2020JD033720, 2021.

Wilcox, E. M.: Stratocumulus cloud thickening beneath layers of absorbing smoke aerosol, Atmospheric Chemistry and Physics, 10, 11769–11777, https://doi.org/10.5194/acp-10-11769-2010, 2010.

Wood, R.: Drizzle in Stratiform Boundary Layer Clouds. Part I: Vertical and Horizontal Structure, https://doi.org/10.1175/JAS3529.1, 2005.

Wood, R. and Bretherton, C. S.: On the Relationship between Stratiform Low Cloud Cover and Lower-Tropospheric Stability, Journal of Climate, 19, 6425–6432, https://doi.org/10.1175/JCLI3988.1, 2006.

Wood, R. and Hartmann, D. L.: Spatial Variability of Liquid Water Path in Marine Low Cloud: The Importance of Mesoscale Cellular Convection, Journal of Climate, 19, 1748–1764, https://doi.org/10.1175/JCLI3702.1, 2006.

Wood, R., Bretherton, C. S., and Hartmann, D. L.: Diurnal cycle of liquid water path over the subtropical and tropical oceans: DIURNAL CYCLE OF LIQUID WATER PATH, Geophys. Res. Lett., 29, 7-1-7–4, https://doi.org/10.1029/2002GL015371, 2002.

~~Yuan, T., Remer~~Zeider, K., McCauley, K., Dmitrovic, S., Siu, L. W., Choi, Y., Crosbie, E. C., DiGangi, J. P., Diskin, G. S., Kirschler, S., Nowak, J. B., Shook, M. A., Thornhill, K. L., Voigt, C., Winstead, E. L., Ziemba, L. D., Zuidema, P., and ~~Yu, H.: Microphysical, macrophysical~~Sorooshian, A.: Sensitivity of aerosol and ~~radiative signatures of volcanic aerosols in trade wind cumulus observed by the A-Train~~cloud properties to coupling strength of marine boundary layer clouds over the northwest Atlantic, Atmospheric Chemistry and Physics, ~~11, 7119–7132~~25, 2407–2422, https://doi.org/10.5194/acp-~~11-7119-2011, 2011~~25-2407-2025, 2025.

Zhang, J~~.~~., Zhou, X., Goren, T., and Feingold, G.~~: Distinct regional meteorological influences on low-cloud albedo~~: Albedo susceptibility ~~over global marine~~ of northeastern Pacific stratocumulus~~ regions~~: the role of covarying meteorological conditions, Atmospheric Chemistry and Physics, ~~23, 1073–1090~~22, 861–880, https://doi.org/10.5194/acp-~~23-1073-2023, 2023~~22-861-2022, 2022.

Zhang, X., Wang, H., Che, H.-Z., Tan, S.-C., Yao, X.-P., Peng, Y., and Shi, G.-Y.: Radiative forcing of the aerosol-cloud interaction in seriously polluted East China and East China Sea, Atmospheric Research, 252, 105405, https://doi.org/10.1016/j.atmosres.2020.105405, 2021.

Zheng, Y., Rosenfeld, D., and Li, Z.: Estimating the Decoupling Degree of Subtropical Marine Stratocumulus Decks From Satellite, Geophysical Research Letters, 45, 12,560-12,568, https://doi.org/10.1029/2018GL078382, 2018.

Zhou, X. and Feingold, G.: Impacts of Mesoscale Cloud Organization on Aerosol-Induced Cloud Water Adjustment and Cloud Brightness, Geophysical Research Letters, 50, e2023GL103417, https://doi.org/10.1029/2023GL103417, 2023.